Published in final edited form as:

Mol Cell. 2023 January 05; 83(1): 43–56.e10. doi:10.1016/j.molcel.2022.12.005.

The FANCJ Helicase Unfolds DNA-Protein Cross-Links to Promote Their Repair

Denitsa Yaneva[1,2,#], **Justin L. Sparks**[3,#], **Maximilian Donsbach**[1,2,#], **Shubo Zhao**[1,2], **Pedro Weickert**[1,2], **Rachel Bezalel-Buch**[4], **Julian Stingele**[1,2,*], **Johannes C. Walter**[3,5,6,*]

[1]Department of Biochemistry, Ludwig-Maximilians-University, 81377 Munich, Germany

[2]Gene Center, Ludwig-Maximilians-University, 81377 Munich, Germany

[3]Department of Biological Chemistry and Molecular Pharmacology, Harvard Medical School, Boston, MA 02115, USA

[4]Department of Biochemistry and Molecular Biophysics, Washington University School of Medicine, Saint Louis, MO, USA

[5]Howard Hughes Medical Institute

[6]Lead Contact

Summary

Endogenous and exogenous agents generate DNA-protein cross-links (DPCs), whose replication-dependent degradation by the SPRTN protease suppresses aging and liver cancer. SPRTN is activated after the replicative CMG helicase bypasses a DPC and polymerase extends the nascent strand to the adduct. Here, we identify a role for the 5' to 3' helicase FANCJ in DPC repair. In addition to supporting CMG bypass, FANCJ is essential for SPRTN activation. FANCJ binds ssDNA downstream of the DPC and uses its ATPase activity to unfold the protein adduct, which exposes the underlying DNA and enables cleavage of the adduct. FANCJ-dependent DPC unfolding is also essential for translesion DNA synthesis past DPCs that cannot be degraded. In summary, our results show that helicase-mediated protein unfolding enables multiple events in DPC repair.

Graphical Abstract

*Correspondence: johannes_walter@hms.harvard.edu, stingele@genzentrum.lmu.de.
#These authors contributed equally

Author Contributions

The project was initiated by J.C.W. and J.L.S, who performed all the experiments in egg extracts. D.Y. and M.D. performed all in vitro reconstitution experiments. S.Z. generated cell lines. P.W. generated reagents and determined formaldehyde sensitivity. R.B-B. purified Pol ζ-Rev1. The work was supervised by J.S. and J.C.W. The manuscript was written by J.L.S, J.S, and J.C.W. with input from all authors.

Declaration of Interests

Johannes Walter is a co-founder of MOMA Therapeutics, in which he has a financial interest.

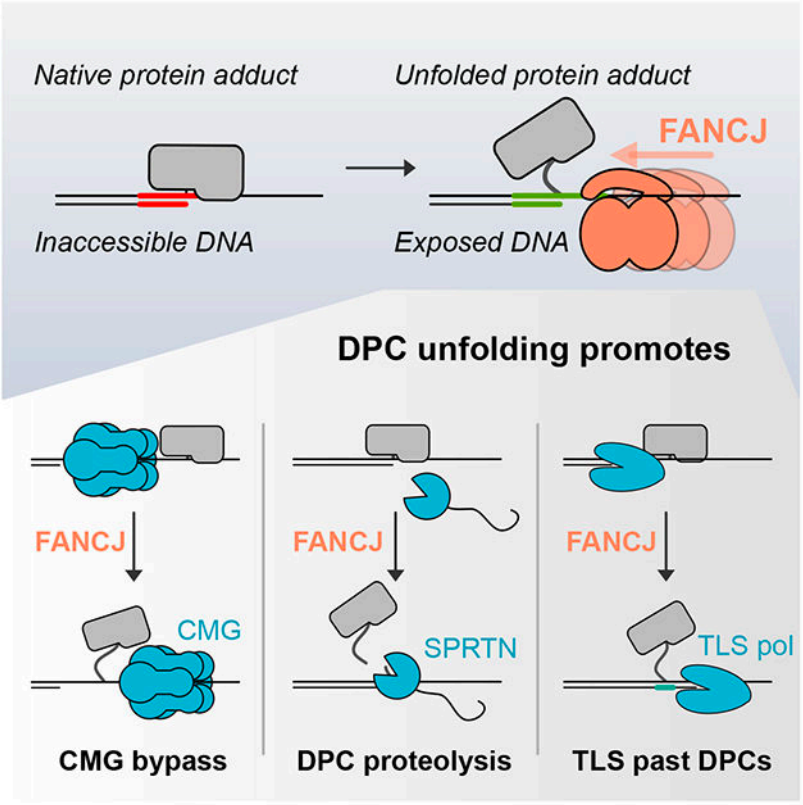

eTOC blurb

When a DNA replication fork encounters a covalent DNA-protein cross-link (DPC), SPRTN cleaves the protein adduct to promote replicative bypass. Yaneva et al. show that the FANCJ helicase promotes SPRTN activity by unfolding the crosslinked protein. DPC unfolding by FANCJ also allows translesion DNA synthesis past non-degradable DPCs.

Introduction

To achieve faithful genome duplication, replisomes overcome myriad obstacles, including DNA-protein cross-links (DPCs) [1,2]. DPCs are generated by UV light, chemotherapeutics, and endogenous agents including abasic sites, formaldehyde, and enzymes such as HMCES and topoisomerases [3]. Experiments in yeast and frog egg extracts identified a pathway of DPC repair that is coupled to DNA replication and involves proteolysis of the protein adduct by a DNA-dependent metalloprotease called Wss1 in yeast and SPRTN in vertebrates [4–6]. This pathway, which is conserved in humans [7–11], does not involve a double-strand break, reducing the risk of gross chromosomal rearrangements. Null mutations in *SPRTN* cause cell death, whereas hypomorphic germline mutations cause Ruijs-Aalfs syndrome, which involves genome instability, progeria, and a susceptibility to hepatocellular carcinoma [12,13]. Thus, SPRTN-dependent DPC repair is critical for cell viability and suppression of human disease.

A model of replication-coupled DPC repair is emerging, primarily from studies in frog egg extracts and in vitro reconstitution [5,6,14–16]. When the replicative CMG helicase collides with a DPC on the leading strand template, the nascent leading strand stalls ~30 nucleotides from the adduct due to the footprint of the CMG helicase (Figure 1A, cartoon), and the E3 ubiquitin ligase TRAIP ubiquitylates CMG. A few minutes after CMG stalls, it resumes translocation and bypasses the intact DPC, which allows extension of the leading strand to within 1 nucleotide of the DPC (Figure 1A; "−1"). CMG bypass depends on the 5' to 3' helicase RTEL1, which translocates along the undamaged lagging strand template and thereby unwinds DNA beyond the lesion. RTEL1 depletion delays but does not abolish CMG bypass, suggesting there could be additional back-up helicases. In human cells, where RTEL1 mutations do not cause formaldehyde sensitivity [17], there might be redundancy among such 5' to 3' DNA helicases, as seen in worms [18]. How CMG can bypass a large adduct on the translocation strand is enigmatic, but we favor the idea that one of the interfaces in the CMG ring opens and allows the DPC to pass through the resulting gap [14]. The single-stranded DNA generated downstream of the DPC recruits the E3 ubiquitin ligase RFWD3, which probably further ubiquitylates the DPC and promotes its destruction by the proteasome, which acts redundantly with SPRTN [6,15].

CMG bypass of the DPC is critical to trigger DPC proteolysis by SPRTN, probably because SPRTN activation depends on the leading strand being extended to within a few nucleotides of the DPC, which can only occur after CMG bypass [6]. In direct support of this idea, purified human SPRTN is most active when a DPC resides near DNA structures bearing single- and double-stranded features including ssDNA-dsDNA junctions [16]. Binding to specific DNA structures likely relieves the autoinhibition of SPRTN's protease domain by its DNA binding domains. Whether any other events or factors are needed to activate SPRTN is unclear.

After DPC proteolysis, the next step in DPC repair is translesion DNA synthesis (TLS), which extends the leading strand past the peptide adduct (Figure 1A; [5]). TLS is a two-step process in which DNA pol η inserts a nucleotide across from the peptide adduct, followed by strand extension beyond the lesion by a complex of REV1 and DNA pol ζ [5,15]. Both steps of TLS depend on RFWD3, whose binding to ssDNA ubiquitylates many proteins in the vicinity of the adduct [15]. Surprisingly, although DPC proteolysis normally precedes TLS, TLS still occurs, albeit slowly, when the DPC cannot be degraded [14]. How a TLS polymerase can accommodate a large, intact DPC in its active site and whether this scenario involves special requirements is unknown.

The fact that CMG bypass is not entirely abolished in the absence of RTEL1 [14] raises the possibility that other 5' to 3' DNA helicases participate in DPC repair. Among the seven vertebrate 5' to 3' DNA helicases, FANCJ is of particular interest. Biallelic mutations in FANCJ cause Fanconi anemia, which is characterized by bone marrow failure, cancer predisposition, and sensitivity to bifunctional agents that induce DNA inter-strand cross-links and DPCs [19]. Current models suggest that FANCJ supports ICL repair primarily by promoting homologous recombination, but its specific role in HR is unknown, and it has not been directly implicated in DPC repair. In apparently distinct functions, FANCJ resolves G4 DNA secondary structures to allow nascent strand progression at the replication fork

([20] and references therein), and it suppresses microsatellite instability[21]. Purified FANCJ displaces DNA binding proteins from DNA[22], but whether this function contributes to DNA replication is unclear. In summary, FANCJ appears to promote diverse genome maintenance pathways that are tied to DNA replication.

Here, we show that the residual DPC bypass and proteolysis observed in RTEL1-depleted egg extracts is further impaired upon co-depletion of FANCJ, demonstrating that FANCJ backs up this function of RTEL1. Similarly, FANCJ cooperates with RTEL1 to help the replisome overcome non-covalent nucleoprotein complexes. Strikingly, FANCJ depletion alone is sufficient to abolish DPC proteolysis by SPRTN, and this function of FANCJ is independent of its role in promoting CMG bypass of the adduct. Normal SPRTN activity is rescued by wild type but not ATPase-deficient FANCJ. In a reconstituted system, FANCJ's ATPase activity is also required for SPRTN-dependent cleavage of DPCs involving DNA binding proteins. In this setting, FANCJ unfolds the protein adduct, which exposes the DNA underlying the DPC while also enabling DPC cleavage by SPRTN. In addition, we find that FANCJ's ability to unfold DPCs promotes TLS past non-degradable protein adducts. Together, our results identify FANCJ-dependent protein unfolding as a central event in replication-coupled DPC repair.

Results

FANCJ backs up RTEL1 for CMG bypass of DPCs

We previously showed that depletion of RTEL1 from egg extracts delays but does not eliminate CMG bypass of DPCs, suggesting that other 5' to 3' helicases might contribute to this process [14]. In addition to RTEL1, vertebrate genomes encode at least six 5' to 3' helicases (FANCJ, DDX11, XPD, PIF1, SETX, and DDX3), and all except DDX11 are detectable on chromatin during DNA replication in *Xenopus* egg extracts [6,14]. To investigate whether these helicases cooperate with RTEL1 to promote CMG bypass, the advance of the leading strand from the −30 position to the −1 position was monitored as a readout of CMG bypass (Figure 1A). Specifically, we replicated pDPC^{Lead} (STAR methods), a plasmid containing a site-specific M.HpaII DPC, in *Xenopus* egg extract depleted of RTEL1 alone or RTEL1 and another 5' to 3' helicase. We included [α-^{32}P]-dATP to label nascent strands. To ensure that the DPC is always encountered on the leading strand template by a single rightward fork, we flanked the DPC with an array of Lac operators bound to Lac repressors (LacRs), which blocks arrival of leftward forks (Figure 1A). To monitor nascent strand synthesis surrounding the DPC, we digested the DNA with AatII and FspI (Figure 1A) and visualized the released, nascent strands using denaturing urea gels and autoradiography. Release of the rightward leading strand by AatII allowed us to track its approach to the DPC; furthermore, the 3' overhangs generated by AatII created fully replicated AatII/FspI lagging strand digestion products that were a few nucleotides longer than the leading strand products, allowing us to distinguish the two (Figure 1A, green vs. red strands). This approach showed that, upon fork collision with the DPC, the nascent leading strands stalled at the −30 position (Figure 1B, lane 1; Figure 1A, left cartoon)[5,14]. CMG then bypassed the intact DPC, allowing extension of the leading strand to the −1 position and progression of the nascent lagging strand past the cross-link, as seen from the appearance of

the larger AatII/FspI product (Figure 1B lanes 2 and 3; Figure 1A, middle cartoon). Arrival of the leading strand at the cross-link triggered DPC proteolysis, and subsequent translesion DNA synthesis (TLS) allowed extension of the nascent leading strand beyond the adduct, as seen from appearance of the smaller AatII/FspI product (Figure 1B, lanes 3-6; Figure 1A, right cartoon)[5,6,14].

Depletion of SETX, PIF1, or DDX3, alone or in combination with RTEL1, had no significant effect on CMG bypass of DPC^{Lead}, as seen from timely extension of the leading strand to the −1 position (data not shown; we did not examine XPD or DDX11). Immunodepletion of FANCJ alone (Figure S1A, lane 3) also did not impact CMG bypass (Figure 1B, lanes 13-18; see graph for quantification). However, depletion of both FANCJ and RTEL1 (Figure S1A, lane 4) led to a substantial further delay in bypass compared to depletion of RTEL1 alone (Figure 1B, lanes 7-12 vs. 19-24). The kinetics of CMG bypass were rescued to the level of RTEL1-only depletion by wild type recombinant FANCJ ($rFANCJ^{WT}$) but not an ATPase deficient FANCJ mutant ($rFANCJ^{K52R}$) (Figure 1B, lanes 25-36; Figure S1A–B). These results show that FANCJ can partially substitute for RTEL1 in promoting CMG bypass of a DPC.

FANCJ backs up RTEL1 in progression through a LacR array

In addition to promoting CMG bypass of DPCs, RTEL1 is required for efficient replisome progression through non-covalent LacR-DNA complexes [14]. To address whether this process also involves FANCJ, we replicated a plasmid containing an array of 12 *lacO* repeats bound by LacR. DNA was recovered at various time points and digested with XmnI, followed by native gel electrophoresis. Replication forks initially converged at the outer edges of the LacR array, generating a discrete X-shaped replication intermediate that was subsequently converted to a linear DNA species when converging forks met (Figure 1C, cartoon and lanes 1-6). As we showed previously, RTEL1 depletion from egg extract slowed the appearance of linear species, indicating its requirement for efficient replisome progression through the LacR array (Figure 1C, lanes 1-6 vs. 7-12; see Figure 1D for quantification; [14]). Immunodepletion of FANCJ from egg extract had no significant effect on accumulation of linear molecules (Figure 1C, lanes 13-18; Figure 1D), but it enhanced the defect seen in RTEL1-depleted extract (Figure 1C, lanes 19-24; Figure 1D). This delay was fully rescued to the level seen in RTEL1-depleted extract by $rFANCJ^{WT}$ but not $rFANCJ^{K52R}$ (Figure 1C, lanes 25-36; Figure 1D). The same result was observed when fork progression was examined at higher resolution using urea PAGE gels (Figure S1C). We conclude that FANCJ backs up RTEL1 to promote efficient helicase progression past covalent and non-covalent proteinaceous barriers.

FANCJ promotes DPC proteolysis

We previously showed that CMG bypass is a prerequisite for efficient DPC proteolysis [14]. Given that FANCJ depletion impairs DPC bypass in RTEL1-depleted extract (Figure 1B), we expected that FANCJ depletion would further compromise DPC proteolysis in the absence of RTEL1. To test this idea, we replicated a plasmid containing two closely-spaced leading strand DPCs (DPC^{Lead}) in extract that was depleted of FANCJ, RTEL1, or both. To monitor degradation of the DPC during DNA replication, we isolated the plasmid,

digested DNA, and blotted for HpaII. We also treated the digested chromatin with the deubiquitylating enzyme Usp21, which collapses ubiquitylated M.HpaII into a single band for easier quantification. As expected [14], DPC degradation was delayed in extracts depleted of RTEL1 (Figure 2A, lanes 1-4 vs. 5-8). Importantly, DPC proteolysis was more severely inhibited in extract co-depleted of RTEL1 and FANCJ (Figure 2A, lanes 13-16). This defect was rescued to the level seen in RTEL1-only depletion by the addition of rFANCJ^{WT} but not rFANCJ^{K52R} (Figure 2A, lanes 17-24). In SPRTN-depleted extract, where the DPC is degraded by the proteasome [6], FANCJ depletion enhanced the proteolysis defect observed in RTEL1-depleted extract, suggesting that FANCJ contributes to a fully functional proteasome pathway (Figure S2A). The same additive effect of combined depletion was observed in extracts supplemented with proteasome inhibitor, implicating FANCJ in SPRTN-mediated DPC destruction (Figure S2B). Thus, in the absence of RTEL1, FANCJ appears to stimulate both sub-pathways of DPC proteolysis.

FANCJ is required for SPRTN activity independently of DPC bypass

To further investigate the involvement of FANCJ in the SPRTN pathway, we examined replication-coupled degradation of a DPC whose lysine residues have been chemically methylated (meDPC). The meDPC cannot undergo ubiquitylation and thus cannot be degraded by the proteasome, but it is still susceptible to SPRTN-mediated degradation, which yields a discrete HpaII fragment (Figure 2B, lanes 1-5)[6,14]. As we reported before, RTEL1 depletion only slightly delayed the appearance of the SPRTN-dependent HpaII fragment, consistent with its partial effect on CMG bypass (Figure 2B, lanes 6-10; [14]). In contrast, FANCJ depletion alone or in combination with RTEL1 depletion abolished SPRTN-dependent meDPC proteolysis (Figure 2B, lanes 11-20), and this defect was reversed by rFANCJ^{WT} but not rFANCJ^{K52R} (Figure 2C). Thus, even in the presence of RTEL1, FANCJ is essential for SPRTN activity.

FANCJ depletion abolished SPRTN activity (Figure 2B) but had no effect on CMG bypass of DPCs (Figure 1B), suggesting that FANCJ promotes SPRTN activity independently of DPC bypass. To test this idea, we exploited the fact that SPRTN can be activated independently of DNA replication or CMG bypass if the DPC is positioned within a ssDNA gap. In this setting, the 3' end flanking the gap was extended towards the DPC, triggering SPRTN activity (Figure 2D, lanes 1-6)[6]. Importantly, FANCJ depletion abolished ssDNA gap-induced SPRTN activity, and the defect was rescued by rFANCJ^{WT} but not rFANCJ^{K52R} (Figure 2D, lanes 7-24). These findings show that FANCJ helicase activity supports SPRTN-dependent DPC proteolysis independently of the replication fork or CMG bypass.

One possible explanation for FANCJ's role in DPC proteolysis is that it recruits SPRTN to the DPC. However, we saw no difference in SPRTN recruitment to the HpaII pDPC in the presence and absence of FANCJ (Figure S2C). Another explanation is that after CMG bypass, FANCJ unwinds DNA secondary structures surrounding the DPC. To test this hypothesis, we flanked the DPC with tracts of thymidines, which should not form any secondary structure. As shown in Figure S2D, FANCJ was still required for SPRTN activity in this context. A third possibility is that RPA binding to the ssDNA surrounding the DPC inhibits SPRTN and that FANCJ removes RPA to relieve this inhibition. However, in the

context of a ssDNA gap substrate, depletion of RPA did not restore meDPC proteolysis in FANCJ-depleted extract (data not shown). We conclude that FANCJ is required for HpaII-DPC proteolysis by SPRTN, independent of FANCJ's role in promoting CMG bypass of the DPC, and not related to SPRTN recruitment, DNA secondary structure disruption, or RPA displacement.

FANCJ is required to promote SPRTN proteolysis of a native DPC

Before exploring further FANCJ's mechanism of action, we addressed whether it promotes proteolysis of an endogenous DPC containing HMCES. HMCES forms DPCs with abasic (AP) sites in ssDNA, which prevents AP site cleavage and formation of double-strand breaks [23]. We recently found that in egg extracts, endogenous HMCES cross-links to the AP site generated when DNA replication triggers ICL unhooking by the NEIL3 DNA glycosylase. In this setting, HMCES is subsequently degraded by SPRTN [24]. A simpler approach to generate a HMCES-DPC involves supplementing egg extract with a plasmid carrying an AP site that resides in a ssDNA gap (Figure 2E [15]). As seen in the context of AP-ICL repair [24], HMCES-DPC proteolysis in this setting was delayed after SPRTN depletion (Figure 2E, lanes 1-12). Importantly, FANCJ depletion delayed HMCES degradation to a similar extent as SPRTN depletion (Figure 2E, lanes 13-18), and the combined depletion of FANCJ and SPRTN did not further stabilize HMCES relative to the single depletions (Figure 2E, lanes 19-24), consistent with FANCJ functioning in the SPRTN pathway. As seen for SPRTN-dependent HpaII destruction, the effect of FANCJ depletion on HMCES proteolysis was rescued by rFANC^{WT} but not rFANCJ^{K52R} (Figure 2F). We conclude that FANCJ is essential for efficient proteolysis of an endogenous HMCES-DPC.

FANCJ is sufficient to promote SPRTN proteolysis of a native DPC

In biochemical reconstitutions, we previously showed that human SPRTN cleaves a protein G-based DPC in the absence of FANCJ or other proteins, as long as the DPC resides near a ssDNA-dsDNA junction [16]. However, most native DPCs involve DNA-binding proteins such as histones [25]. To investigate how FANCJ affects proteolysis of a native DPC, we used human proteins to reconstitute proteolytic repair of a DPC formed by the catalytic SRAP-domain of HMCES, which interacts tightly with the underlying DNA [26,27]. We incubated HMCES^{SRAP} with an AP site-containing oligonucleotide to form a HMCES^{SRAP}-DPC (Figure 3A, lane 3 and Figure S3A) [23]. Strikingly, unlike the protein G-DPC, the HMCES^{SRAP}-DPC was degraded by SPRTN only in the presence of FANCJ and ATP (Figure 3A, lanes 4-7, Figure 3B for quantification). Efficient proteolysis depended on the presence of a ssDNA-dsDNA junction (Figure S3B, compare lanes 6 and 12, Figure S3C for quantification). While we were unable to test a human FANCJ ATPase mutant in our assays due to aggregation of the recombinant protein (FANCJ-K52R, data not shown), a requirement for FANCJ's ATPase activity was indicated by the inability of frog rFANCJ^{K52R} to support DPC cleavage (Figure S3D). In addition, we tested a Fanconi anemia-causing FANCJ patient variant (FANCJ-A349P), which hydrolyzes ATP and translocates on ssDNA but fails to produce enough force to unwind DNA structures, such as G4 quadruplexes [28]. FANCJ-A349P did not support SPRTN activity (Figure 3A, lanes 8-10), suggesting that force generation by FANCJ's ATPase motor is required for DPC cleavage. While a prior study showed that RPA stimulates FANCJ's ability to displace

proteins from DNA [22], FANCJ's stimulation of SPRTN activity was not affected by low concentrations of RPA, whereas high concentrations were inhibitory (Figure S3E). These results suggest that the requirement for FANCJ in DPC proteolysis is conserved in humans and involves a direct collaboration between the motor activity of FANCJ and SPRTN.

FANCJ unfolds the protein adduct

We speculated that FANCJ promotes SPRTN activity by translocating into the DPC, which remodels the protein adduct. To test this idea, we asked whether disrupting the native conformation of the protein adduct would bypass the requirement for FANCJ. We first heat-denatured the DPC before adding SPRTN, but this led to only a low level of DPC cleavage in the absence of FANCJ (Figure 4A, lane 12, red arrow). As an independent approach to destabilize the DPC, we generated a HMCES^{SRAP}-DPC with reduced DNA-binding activity. We utilized a previously described HMCES^{SRAP} R98E variant, which shows almost no activity in DNA gel-shifts but forms DPCs, implying significant residual DNA binding (Figure S4A and S4B) [23]. As seen for HMCES^{SRAP}-WT (Figure 4A, lanes 7-8), HMCES^{SRAP}-R98E was only cleaved in the presence of active SPRTN and FANCJ (Figure 4A, compare lanes 20 and 23-24). However, upon heat-denaturation, the mutant DPC was cleaved efficiently in the absence of FANCJ (Figure 4A, lanes 28 vs 31). We speculated that the mutant adduct remained denatured following heat treatment while the WT adduct refolded. To test this possibility, we analyzed WT and mutant HMCES^{SRAP}-DPCs by native PAGE before and after heat treatment. Prior to denaturation, both DPCs entered the gel (Figure S4C, lanes 3 and 4 and Figure S4D for quantification). In the case of WT HMCES^{SRAP}, a noncovalent complex between the DPC and free HMCES^{SRAP} was also observed (Figure S4C, lane 3). Following heat treatment, the majority of WT DPCs still entered the gel and migrated at the original position, consistent with a native conformation (although the noncovalent complexes disappeared). In contrast, HMCES^{SRAP} R98E-DPCs remained in the well, indicating a non-native, misfolded state (Figure S4C, compare lanes 7 and 8). Our data demonstrate that cleavage of a DPC formed between a native DNA binding protein and DNA requires FANCJ, whereas when such a DPC is unfolded, FANCJ is dispensable.

To test directly whether FANCJ unfolds the DPC, we probed the conformation of the protein adduct using limited proteolysis. The native WT and R98E HMCES^{SRAP}-DPC displayed one major tryptic cleavage site (Figure 4B, lanes 4-6 and 17-19, green arrow). Remarkably, addition of FANCJ exposed additional tryptic cleavage sites in native WT and R98E HMCES^{SRAP}-DPCs very close to the DNA (Figure 4B, lanes 7-9 and 20-22, orange arrows). No effect was observed in the absence of ATP or upon addition of the patient variant FANCJ-A349P (Figure S4E). The same tryptic cleavage sites were exposed upon heat-denaturation of the R98E HMCES^{SRAP}-DPC (Figure 4B, lanes 2426, orange arrows), but not the WT HMCES^{SRAP}-DPC (Figure 4B, lanes 11-13), which confirms that the WT adduct retains a native conformation upon heat-denaturation. We conclude that FANCJ partially or completely unfolds the protein adduct.

FANCJ exposes DNA underlying the DPC

We next asked whether unfolding of the protein adduct exposes the underlying DNA. To this end, we placed a HaeIII-restriction enzyme site in the dsDNA 1 nucleotide from the HMCES^{SRAP}-protein adduct (Figure 5A). HaeIII cleaved the free DNA, but failed to do so upon DPC formation, suggesting that the protein adduct blocked access of the restriction enzyme (Figure 5A, compare lanes 1-2 with 5-6). In this setting, FANCJ restored HaeIII cleavage in an ATP-dependent manner (Figure 5A, lanes 7-9), and, as seen for SPRTN activity, the requirement for FANCJ was bypassed by heat denaturation of the HMCES^{SRAP} R98E-DPC (Figure S5A). In contrast, a HaeIII-site placed 8 nucleotides away from the DPC was efficiently cleaved independently of FANCJ (Figure 5A, lanes 14-17). Together, these experiments suggest that FANCJ-dependent DPC unfolding exposes the DNA beneath the DPC, which might allow SPRTN to bind the ssDNA-dsDNA junction and undergo activation. To test whether providing DNA access is sufficient for DPC cleavage, we placed the ssDNA-dsDNA junction adjacent to the DPC footprint, 8 nucleotides from the cross-linking site (SPRTN cleaves protein G adducts up to 10 nucleotides away from an activating structure [16]). At this position, the ssDNA-dsDNA junction was fully accessible, as indicated by efficient HaeIII cleavage (Figure 5B, lanes 7-9). However, cleavage of the HMCES^{SRAP}-DPC by SPRTN was only observed upon addition of FANCJ or heat denaturation of the R98E mutant variant (Figure 5B, lanes 10-12, and Figure S5B). This result indicates that DPC unfolding is required even when the ssDNA-dsDNA junction is accessible and raises the question why the motor activity of FANCJ is not required for protein G-DPC proteolysis. To address this, we tested the conformation of the protein G adduct using limited proteolysis. Strikingly, we observed a major tryptic cleavage site very close to the DNA that was independent of FANCJ (Figure S5C), suggesting that a flexible, unstructured part of protein G near the attachment site is available for SPRTN cleavage. In summary, our data show that FANCJ-dependent DPC unfolding exposes the underlying DNA, which might allow SPRTN to bind and undergo de-repression of its protease domain. However, in the context of structured DPCs, FANCJ is still required even when an activating DNA structure is accessible, probably to unfold the DPC and allow its entry to the narrow SPRTN active site.

FANCJ is required to promote translesion synthesis past stable DPCs

Once a DPC has undergone proteolysis, the remaining peptide adduct is bypassed by TLS, which leads to recoupling of the leading strand with CMG (Figure 1A). However, we previously showed that even when a DPC fails to be degraded (e.g. due to SPRTN depletion and DPC methylation), TLS can still extend the nascent leading strand past the intact adduct, albeit more slowly than usual, as seen from the large accumulation of −1 species (Figure 6A, lanes 1-6 vs. 13-18)[14]. Strikingly, FANCJ depletion abolished TLS past the meDPC in SPRTN-depleted extract, permanently arresting the leading strand at the −1 position and preventing accumulation of the mature leading strand product (Figure 6A, lanes 19-24). By contrast, TLS was independent of FANCJ when the DPC was unmethylated and could therefore be ubiquitylated and degraded by the proteasome (Figure 6A, lanes 7-12; Figure 1A). Furthermore, when the DPC was pre-digested to a short peptide using proteinase K, TLS still depended on Rev1 [6] but was independent of FANCJ (Figure 6B, lanes 11-20). These results indicate that FANCJ is not a general TLS factor, but rather is crucial at large

protein adducts that cannot be degraded. Our results support the idea that DPC proteolysis normally precedes TLS, but if DPC proteolysis fails, FANCJ promotes TLS past the intact DPC.

We next addressed whether FANCJ is also required for TLS when a stable DPC is located in a ssDNA gap [6]. In this setting, FANCJ depletion also greatly inhibited TLS, and we observed that during extension, the 3'-end flanking the gap initially stalled at the −3 position, followed by slow progression to −1 (Figure 6C, lanes 8-14). TLS and the efficient approach to −1 were restored by rFANC^{WT} but not rFANCJ^{K52R} (Figure 6C, lanes 15-28). Similarly, loss of FANCJ also caused nascent leading strands to arrest further away from the DPC in the context of full replisome collision with the adduct (Figure 1B, lanes 13-18, pink arrowhead). These stalling products disappeared upon addition of rFANC^{WT} but not rFANCJ^{K52R} (Figure 1B, lanes 25-36).

To address whether these effects stem from a direct role of FANCJ in promoting TLS at a DPC, we cross-linked the HMCES^{SRAP} domain downstream of a primer template junction and added human Pol η or yeast Pol ζ-Rev1 polymerase with and without FANCJ. In the absence of FANCJ, Pol η failed to bypass the HMCES^{SRAP}-DPC, and was unable to advance efficiently to the cross-linking site (Figure 6D, compare lanes 1, 4, and 5), consistent with our observations in egg extracts. Addition of FANCJ WT but not of FANCJ-A349P facilitated advance of the polymerase towards the lesion, but no bypass synthesis was observed (Figure 6D, lane 6-9). Similar to Pol η, Pol ζ-Rev1 failed to advance to the cross-linking site. However, in the presence of FANCJ, Pol ζ-Rev1 efficiently extended the primer past the intact DPC (Figure 6E, lanes 6-9); combining Pol ζ-Rev1 and Pol η did not result in synergistic effects (data not shown). We propose that FANCJ-dependent unfolding of the DPC allows leading strands to advance towards and eventually bypass the large protein adduct.

Discussion

Our results suggest a central role for FANCJ in replication-coupled DPC repair (Figure 7). After CMG stalls, RTEL1 unwinding past the DPC creates a stretch of ssDNA downstream of the adduct. FANCJ binds to this ssDNA and translocates back towards the adduct, which it unfolds, thereby facilitating DPC proteolysis by SPRTN, TLS past non-degradable DPCs, and possibly CMG bypass. To our knowledge, protein unfolding by DNA-dependent ATP motors has not been described.

The role of FANCJ in SPRTN activity

In reconstitution experiments, SPRTN is sufficient to cleave a protein G-DPC [16], but cleavage of a HMCES^{SRAP}-DPC requires the ATPase activity of FANCJ, as does destruction of HpaII in egg extracts. Critically, HpaII and the SRAP domain are tightly folded and bind DNA intimately [26,29], whereas the protein G construct we used has no DNA binding activity and contains an unstructured His-tag adjacent to the attachment site. These findings suggested that the motor activity of FANCJ might unfold cross-linked DNA binding proteins and thereby promote SPRTN activity. Consistent with this model, FANCJ's ATPase activity enhanced HMCES^{SRAP}-DPC proteolysis by trypsin, and when

the DPC was irreversibly unfolded (through a combination of a point mutation and heat denaturation), the requirement for FANCJ in SPRTN activity was abrogated. Moreover, a clinically relevant FANCJ mutation (A349P) that specifically disrupts FANCJ's ability to convert ATP hydrolysis to force generation [28] inhibited SPRTN activation by FANCJ. We envision at least two mechanisms by which DPC unfolding promotes SPRTN activity. First, unfolding allows SPRTN binding to the ssDNA-dsDNA junction, promoting SPRTN de-repression. Consistent with this idea, unfolding exposes DNA in the immediate vicinity of the DPC. Second, unfolding allows the DPC to access SPRTN's narrow active site cleft[30]. Consistent with this idea, DPC unfolding is important even when the activating DNA structure is placed adjacent to the DPC. Future work will be required to test these models more directly.

FANCJ promotes translesion DNA synthesis past stable DPCs

In unperturbed DPC repair reactions, DPC proteolysis precedes TLS [5], and when DPC proteolysis is blocked, TLS is delayed [14] but now depends absolutely on FANCJ. These data show that DPC proteolysis normally facilitates TLS, but that in the absence of proteolysis, TLS can still proceed with the assistance of FANCJ. When we prevented DPC proteolysis in the context of the gapped substrate, leading strands stalled at the −1 position before undergoing TLS, whereas in the absence of FANCJ, they first stalled at the −3 position, before permanently arresting at the −1 position (Figure 6C). This result shows that in the context of an intact DPC, FANCJ is critical for approach to the −1 position. Similarly, in reconstituted reactions, FANCJ enabled Pol ζ-Rev1 to not only approach a DPC, but also to synthesize across the lesion. We propose that FANCJ-dependent unfolding of the protein adduct enables polymerase approach by reducing the footprint of the DPC, and that it enables extension by allowing the bulky protein adduct to access the polymerase active site.

FANCJ helps CMG overcome obstacles

Our data show that FANCJ is partially redundant with RTEL1 in allowing CMG to bypass DPCs, and in promoting replisome progression through a LacR array. In the case of DPC bypass, we propose that FANCJ partially substitutes for RTEL1 in unwinding DNA beyond the DPC via translocation on the lagging strand template. The fact that FANCJ depletion alone has no effect on CMG bypass suggests that DPC unfolding is not essential for CMG bypass, or that FANCJ functions redundantly with other factors in this step of DPC repair. In the case of replisome progression through LacR arrays, we propose that like RTEL1, FANCJ cooperates with CMG in the disruption of these non-covalent nucleoprotein complexes by translocating on the lagging strand template. Alternatively, or in addition, FANCJ might disrupt LacR complexes by functioning on the leading strand template *behind* CMG. Thus, after passage of CMG beyond a LacR-*lacO* complex and extension of the leading strand to the *lacO* site, pol ε might dissociate, allowing LacR to re-bind. The re-formed LacR-*lacO* complex would prevent further progression of the leading strand and cause limited CMG uncoupling. Analogous to its function in DPC repair, FANCJ might then bind to the ssDNA downstream of *lacO* on the leading strand template and motor back to displace LacR. Translocation of FANCJ into the tightly bound protein would either displace LacR directly, or unfold LacR, disrupting its interaction with DNA.

Limitations of this study

How a DNA-dependent translocase such as FANCJ unfolds protein adducts, and whether DPCs are unfolded partially (as depicted in Figure 7) or completely, remain exciting open questions. Another important question is whether FANCJ regulates DPC repair in cells. Notably, *FANCJ* was identified as the second-strongest hit in genome-wide screens for formaldehyde sensitivity in RPE1 cells [17]. In agreement, we found that knocking out the *FANCJ* gene in U2OS cells resulted in formaldehyde sensitivity, which was complemented by re-expression of wildtype enzyme but not by FANCJ-K52R or FANCJ-A349P (Figure S6). However, unlike *SPRTN* knockouts, *FANCJ* knockouts are viable. Although this could indicate that FANCJ does not support SPRTN activity in mammals, our biochemical reconstitutions with human SPRTN and FANCJ suggest otherwise. More likely, another 5' to 3' helicase is redundant with FANCJ. Consistent with a dedicated role for FANCJ in DPC repair, FANCJ knockouts are more sensitive to formaldehyde than knockouts in other FANC genes [17], and double knockouts of FANCJ and FANCD2 display added sensitivity towards crosslinking agents [21]. Interestingly, mutations in SPRTN, FANCJ, and RTEL1, all of which function in DPC repair in egg extracts, have different phenotypes in humans [12,19,31]. This could be due to the fact that these proteins, especially the helicases, have numerous functions, and that hypomorphic human mutations probably cause a partial loss in a subset of these functions. Understanding the precise role of FANCJ and other proteins in human DPC repair, and how their dysfunction causes disease is an important future goal.

Conclusion

Together with recent work on FANCJ-dependent resolution of G4 quadruplexes [20,32], our results suggest a general model for the action of FANCJ in overcoming replicative obstacles. When CMG stalls at a major barrier on the leading strand template (such as a DPC or G4), an accessory helicase unwinds DNA beyond the barrier. This can involve RTEL1 translocating 5' to 3' along the lagging strand template to facilitate bypass of DPCs, or DHX36 translocating 3' to 5' along the leading strand template to facilitate bypass of G4s. FANCJ then loads onto the unwound leading strand template and translocates back towards the obstacle, on which it exerts force. FANCJ thereby unfolds the barrier, allowing protease activity, and/or leading strand extension past the obstacle. We identify FANCJ-mediated unfolding of DPCs and other obstacles as a versatile new function in the DNA repair toolbox.

STAR Methods

RESOURCE AVAILABILITY

Lead Contact—Further information and requests for resources and reagents should be directed to and will be fulfilled by the Lead Contact, Johannes C. Walter (johannes_walter@hms.harvard.edu).

Materials Availability—All plasmids are available on request.

Data and Code Availability

- Original western blot and gel images reported in this paper have been deposited at Mendeley and are publicly available as of the date of publication. The DOI is listed in the key resources table.
- This study did not generate original code.
- Any additional information required to reanalyze the data reported in this paper is available from the lead contact upon request.

EXPERIMENTAL MODEL AND SUBJECT DETAILS

Xenopus laevis—Egg extracts were prepared using *Xenopus laevis* (Nasco Cat #LM0053MX). All experiments involving animals were approved by the Harvard Medical Area Institutional Animal Care and Used Committee and conform to relevant regulatory standards.

Insect cell lines—Sf9 cells (Expression Systems Cat# 94-001S) were cultured at 27 °C for protein overexpression. Cells were cultured in ESF 921 insect cell culture medium (Fisher Scientific Cat#96-001-01-CS).

Mammalian cell lines—U2OS T-REx Flp-ln cells were provided by Cell Services, The Francis Crick Institute, and grown in Dulbecco's Modified Eagle Medium (DMEM) supplemented with 10% (v/v) fetal bovine serum (FBS).

METHODS DETAILS

Preparation of DNA constructs—To generate pDPC plasmids, either pJLS2 or pJLS3 were nicked with Nt.Bbvcl (DPC^{Lead}) and ligated with an oligonucleotide containing a fluorinated cytosine (dFdC_Jead; sequences provided in Supplementary Table S1) and subsequently cross-linked to M.HpaII-His_6 or methylated M.HpaII-His_6 to generate $pDPC^{Lead}$ and $pDPC^{2xLead}$ or $pmeDPC^{Lead}$ and $pmeDPC^{2xLead}$, respectively, as previously described [5]. Creation of $pDPC^{ssDNA}$ and $pmeDPC^{ssDNA}$ was previously described [6]. Briefly, pJLS2 was nicked with Nb.Bbvcl and ligated with an oligonucleotide containing a fluorinated cytosine (dFdC_bottom). The dFdC-containing plasmid was then nicked with Nt.Bbvcl and the resulting 31 bp fragment was melted and captured by annealing with an excess of the complementary oligo (Top_capture). Remaining oligos were then degraded by Exonuclease I (New England BioLabs) treatment. The gapped plasmid was subsequently cross-linked to M.HpaII-His_6 or methylated M.HpaII-His_6 to generate $pDPC^{ssDNA}$ or $pmeDPC^{ssDNA}$, respectively, as previously described [5]. The C5-Fluor dC modified plasmids were mixed with either methylated M.HpaII or nonmethylated M.HpaII in M.HpaII reaction buffer (50 mM Tris-HCl, pH 7.5, 5 mM 2-mercaptoethanol, 10 mM EDTA) and supplemented with 100 mM S-adenosylmethionine (NEB, Ipswich, MA) for 12-18 hours at 37 °C. Creation of pAP^{ssDNA} plasmid was previously described [15]. Briefly, pJLS2 was nicked with Nb.Bbvcl and ligated with an oligonucleotide containing a uracil (dUdC_bottom). The dU-containing plasmid was then nicked with Nt.Bbvcl and the resulting 31 bp fragment was melted and captured by annealing with an excess of the

complementary oligo (Top_capture). Remaining oligos were then degraded by Exonuclease I (New England BioLabs) treatment. The gapped plasmid was subsequently in experiments.

Xenopus* egg extracts and DNA replication—Xenopus* egg extracts were prepared as described [34]. Briefly, licensing was carried out by supplementing a high-speed supernatant (HSS) of egg cytoplasm with plasmid DNA at a final concentration of 7.5–15 ng/μL. For radiolabeling DNA replication products, [α-^{32}P]-dATP was added to HSS prior to the DNA. For replication in the presence of LacI, 1 volume of plasmid (75 ng/μL) was incubated with an equal volume of 12 μM LacI for 30 minutes prior to transfer into HSS so that the final concentration of plasmid was 7.5 ng/μl [5]. Licensing mixes were incubated for 30 min at room temperature to assemble pre-replicative complexes (pre-RCs). To prevent licensing, Geminin was added to HSS at a final concentration of 10 μM and incubated for 10 min at room temperature prior to addition of plasmid DNA. To initiate replication, 1 volume of licensing reaction was mixed with 2 volumes of nucleoplasmic extract (NPE) that had been diluted two-fold with 1xELB-sucrose (10 mM Hepes-KOH pH 7.7, 2.5 mM $MgCl_2$, 50 mM KCl, 250 mM sucrose). 0.5 μl aliquots of replication reaction were typically stopped with 5–10 volumes of replication stop buffer (8 mM EDTA, 0.13% phosphoric acid, 10% ficoll, 5% SDS, 0.2% bromophenol blue, 80 mM Tris-HCl at pH 8), treated with 1 μg/μL Proteinase K. For nascent strand analysis, 2.5 μl aliquots of replication reaction were stopped in 10 volumes of sequencing stop buffer (0.5 % SDS, 25 mM EDTA, 50 mM Tris-HCl pH 8.0) followed by addition of 1.25 μl of 190 ng/μL RNase A and incubated for 30 minutes at 37 °C. After RNase digestion, 1.25 μl of 900 ng/μL Proteinase K was added to the DNA samples and incubated overnight at room temperature. Following the Proteinase K treatment, samples were diluted to 150 μl with 10 mM Tris-HCl pH 8.0. The samples were extracted once with an equal volume of phenol/chloroform followed by one extraction with an equal volume of chloroform. The DNA was then precipitated with the addition of 0.1 volumes 3M sodium acetate pH 5.2 and 1 μl glycogen (20 mg/ml stock) and resuspended in 7.5 μl of 10mM Tris-pH 7.5. For RTEL1 immunodepletion and rescue experiments, NPE was supplemented with ~ 200 nM recombinant wild type or mutant *Xenopus* RTEL1 and incubated for 15 minutes prior to replication initiation. For MG262 (stock 20 mM; Boston Biochem. Cat# I-120) treatment, NPE was supplement with 200 μM MG262 and incubated for 15 minutes prior to mixing with HSS (133.33 μM final concentration in replication mix). Samples were analyzed by native 0.8% agarose gel electrophoresis. Gels were exposed to phosphorscreens and imaged on a Typhoon FLA 7000 phosphorimager (GE Healthcare). Band or total lane intensities were quantified using Multi-Gauge software (Fujifilm) with subtraction of appropriate background.

Nascent strand analysis—To nick radio-labeled nascent leading-strands, 3-4 μl of extracted and ethanol precipitated DNA at 1-2 ng μl^{-1} was incubated in 1x outsmart buffer (New England BioLabs) with 0.45 units μl^{-1} Nt.BspQI (New England BioLabs) in a 5 μl reaction at 37 °C for 2 h. Nicked DNA (3.5 to 4 μl samples) was separated on 4% polyacrylamide sequencing gels. To digest radio-labeled nascent leading-strand 3-4 μl of extracted and ethanol precipitated DNA a 1-2 ng μl^{-1} was incubated in 1x cutsmart buffer (New England BioLabs) with 1 unit μl^{-1} AatII (New England BioLabs) and FspI (New England BioLabs) in a 5 μl reaction at 37 °C for 2 h. Digestion reactions were

stopped with 0.5 volumes of Sequencing Stop solution (95% formamide, 20 mM EDTA, 0.05 % bromophenol blue, 0.05% xylene cyanol FF). Digested DNA (3.5 to 4 μl samples) was separated on 7% polyacrylamide sequencing gels. Gels were dried and subjected to phosphorimaging using a Typhoon FLA 7000 phosphoimager. Gels were quantified using Multi Gauge software (Fujifilm).

To quantify the percentage of CMG that underwent bypass, the radioactive signal of all leading strands located between positions +1 and −29 on the gel (reflecting CMGs that have bypassed) was divided by the radioactive signal for leading strands between positions +1 and −44 (reflecting CMGs that have stalled at the lesion or undergone bypass). To help visualize bands, brightness and contrast of some scanned gels were adjusted globally using ImageJ. Quantification of radioactive gels was performed using Typhoon imaging software.

Antibodies and immunodepletion—The xlFANCJ-N antibody was raised against amino acids 69-249 of *Xenopus laevis* FANCJ [35]. FANCJ antibody was affinity purified from serum using the FANCJ antigen according to standard protocols. In Western blotting of NPE, the affinity-purified xlFANCJ-N antibody recognized ~160 and ~140 kD bands (data not shown). Both bands were immunoprecipitated from NPE by affinity-purified xlFANCJ-N antibody, but this antibody partially co-depleted FANCM and FANCA (data not shown). The xlFANCJ-C antibody was raised against a C-terminal peptide of FANCJ (CNRENRLSRSRNKGVSSFFLD) by Bethyl laboratories, and it specifically recognized the 160 kD FANCJ band without appreciably co-depleting the 140 kD FANCJ band, which we infer is a C-terminal truncation. It also did not co-precipitate FANCA or FANCM (data not shown). The following antibodies were described previously: RTEL1-N [14], CDC45 [36], M.HpaII [6], PSMA3 [6], SPRTN-N [6], Histone H3 (Cell Signaling Cat #9715S), Mcm6 [14], and HMCES [24].

For FANCJ immunodepletion, 4 volumes of purified xlFANCJ-N, xlFANCJ-C antibody (1 mg mL^{-1}), or an equivalent amount of rabbit IgG purified from non-immunized rabbit serum (Sigma) were incubated with 1 volume of Protein A Sepharose Fast Flow (PAS) (GE Healthcare) overnight at 4°C. For RTEL1 immunodepletion, 3.5 volumes of purified RTEL1 antibody (1 mg mL^{-1}) or an equivalent amount of rabbit IgG purified from non-immunized rabbit serum (Sigma) were incubated with 1 volume of Protein A Sepharose Fast Flow (PAS) (GE Healthcare) overnight at 4°C. For SPRTN immunodepletion, 4 volumes of SPRTN serum was incubated with 1 volume of Protein A Sepharose Fast Flow (PAS) (GE Healthcare) overnight at 4°C. For mock depletion, 4 volumes of preimmune serum from matched rabbit, was used. In each case, one volume of antibody-conjugated Sepharose was added to 5 volumes of precleared HSS or NPE and incubated for 1 hour at 4°C. The HSS or NPE was collected and incubated two more times with antibody-conjugated sepharose for a total of three rounds of depletion. The depleted HSS or NPE was collected and used immediately for DNA replication, as described above. For FANCJ immunodepletions, xlFANCJ-C antibody was used for the first round of depletion, and the xlFANCJ-N antibody was used for the second and third rounds of depletion. This procedure avoided significant co-depletion of FANCM and FANCA. We speculate that these proteins interact with the C-terminus of the 160 kD form of FANCJ, and that they are displaced from FANCJ by the C-terminal antibody during the first round of depletion.

Protein expression and purification—M.HpaII-His_6, LacI-biotin, and LacI-His_6 were expressed and purified as previously described [5]. Lysine methylation of M.HpaII was carried out as described [6]. *Xenopus* FANCJ open reading frame with an N-terminal FLAG tag separated by a 3C cleavage site was cloned into pFastBac1 (Thermo Fisher Scientific) (pJLS102) using custom gene synthesis from Integrated DNA Technologies (IDT). The FANCJ sequence was confirmed by Sanger sequencing. FANCJ-K52R mutant was created by around-the-horn site-directed mutagenesis, and mutations were confirmed by Sanger sequencing. The FLAG-FANCJ Baculoviruses were created using the Bac-to-Bac system (Thermo Fisher Scientific) according to the manufacturer's protocols. FLAG-FANCJ and mutants were expressed in 3 L suspension cultures of Sf9 cells (Thermo Fisher Scientific) by infection with FANCJ baculovirus for 36-48 hrs. Sf9 cells were collected via centrifugation and washed with 1X PBS and subsequently pelleted by centrifugation and flash frozen. Cell pellets were thawed and resuspended in 2 volumes of 1.33X Lysis Buffer (33.33 nM HEPES pH 7.5, 550 M NaO_2Ac, 13 % sucrose, 0.1 % IGEPAL, 1.33X Roche EDTA-free Complete protease inhibitor cocktail), 1X Lysis Buffer (25 mM HEPES pH 7.5, 400 mM NaO_2Ac, 10 % sucrose, 0.075 % IGEPAL, 1X Roche EDTA-free Complete protease inhibitor cocktail) to the weight of the cell pellet. Cells were lysed by sonication, and the lysate was cleared by ultracentrifugation at 25,000 rpm in a Beckman Ti45 rotor for 1 hour. The supernatant was incubated for 2 hours with preequilibrated ANTI-FLAG M2 Affinity Gel (Sigma) at 4 °C. Following incubation, resin was first washed with $Wash\ Buffer_{400}$ (25 mM HEPES pH7.5, 400 mM NaO_2Ac, 10 % sucrose, 0.01% IGEPAL, 1X Roche EDTA-free Complete protease inhibitor cocktail) and then with $Wash\ Buffer_{200}$ (25 mM HEPES pH7.5, 200 mM NaO_2Ac, 10 % sucrose, 0.01 % IGEPAL). Proteins were eluted from the resin with $Elution\ Buffer_{200}$ (25 mM HEPES pH7.5, 200 mM NaO_2Ac, 10 % sucrose, 0.005 % IGEPAL, 0.2 mg/ml 3XFLAG peptide). Fractions were pooled and dialyzed against Dialysis Buffer (25 mM HEPES pH7.5, 200 mM NaO_2Ac, 10 % sucrose, 0.005 % IGEPAL, 2 mM DTT) with addition of HRV 3C protease (Thermo Fisher) at 4°C for 4 hr to remove FLAG tag. Following dialysis, the protein sample was diluted to 100 mM sodium acetate using dilution buffer (25 mM HEPES pH7.5, 0 mM NaO_2Ac, 10 % sucrose, 0.005 % IGEPAL, 2 mM DTT). The protein sample was then incubated with preequilibrated Nuvia S resin (Biorad) rotating for one hour at 4 °C. The resin was collected by centrifugation and resin washed with $Wash\ Buffer_{150}$ (25 mM HEPES pH7.5, 150 mM NaO_2Ac, 10 % sucrose, 0.005 % IGEPAL, 2 mM DTT). FANCJ was eluted with $Elution\ Buffer_{400}$ (25 mM HEPES pH7.5, 400 mM NaO_2Ac, 10 % sucrose, 0.005 % IGEPAL, 2 mM DTT). Aliquots were flash frozen and stored at −80°C.

An open reading frame of human FANCJ codon-optimized for expression in insect cells followed by a TwinStrep tag and separated by a TEV-cleavage site was obtained by custom gene synthesis (GeneArt) and cloned into pFastBac1. FANCJ Baculoviruses were created using the Bac-to-Bac system (Thermo Fisher Scientific) according to the manufacturer's protocols. FANCJ-TwinStrep was expressed in 4 L suspension cultures of Sf21 cells (Thermo Fisher Scientific) by infection with FANCJ baculovirus for 72 hrs. Sf21 cells were collected via centrifugation and lysed in 200 mL of Lysis Buffer (50 mM Tris-HCl pH 8, 500 mM KCl, 0.1% Triton X-100, 10 mM $MgCl_2$, Benzonase nuclease, cOmplete EDTA-free protease inhibitor cocktail tablets, 1 mM DTT) with a Microfluidizer (3x). The lysate

was cleared by ultracentrifugation at 40,000 rpm in a Beckman Ti45 rotor for 45 minutes. The supernatant was loaded overnight on a 5 ml Strep-Tactin® XT 4Flow®cartridge using a sample pump. The proteins were eluted from the column with Strep Elution Buffer (50 mM Tris-HCl pH 8, 500 mM KCl, 0.1% Triton X-100, 50 mM biotin, 1 mM DTT). Fractions were pooled and dialyzed overnight at 4°C against Dialysis Buffer (50 mM Tris-HCl pH 8, 150 mM KCl, 1 mM DTT) with addition of His-TEV protease to remove the TwinStrep tag. Following dialysis, the protein sample was loaded on a 1 mL HiTrap® Heparin HP affinity column equilibrated in Dialysis Buffer, and eluted in a gradient of Heparin Elution Buffer (50 mM Tris-HCl pH 8, 1 M KCl, 1 mM DTT). Fractions were pooled, concentrated to 1 mL and further purified by size exclusion chromatography using a Superdex® 200 Increase 10/300 GL column equilibrated in Equilibration Buffer (25 mM HEPES/KOH pH 7.5, 200 mM KCl, 10% Glycerol, 1 mM TCEP). Eluted proteins were concentrated, snap-frozen in liquid nitrogen and stored at −80°C.

For experiments shown in Figures 3A, 6D, 6E, and S4E, FANCJ WT and FANCJ-A349P were purified using an optimized strategy. To this end, a Z-basic tag was inserted C-terminally of FANCJ in pFastBac1 plasmid (FANCJ-A349P was generated using site-directed mutagenesis). FANCJ-WT and -A349P Baculoviruses were created using the Bac-to-Bac system (Thermo Fisher Scientific) according to the manufacturer's protocols. FANCJ-Z-basic-TwinStrep-WT and –A349P were expressed in 4 L suspension cultures of Sf21 cells (Thermo Fisher Scientific) by infection with FANCJ baculovirus for 72 hrs. Sf21 cells were collected via centrifugation and lysed in 200 mL of Lysis Buffer (50 mM Tris-HCl pH 8, 500 mM KCl, 0.1% Triton X-100, 10 mM $MgCl_2$, smDNAse nuclease, 0.04 mg/mL Pefabloc SC, cOmplete EDTA-free protease inhibitor cocktail tablets, 1 mM TCEP) with a Dounce homogenizer (25x). The lysate was cleared by centrifugation at 20,000 rpm in a Beckman JA-25.50 rotor for 2 hrs. The supernatant was loaded on a 5 ml Strep-Tactin® XT Superflow® high-capacity cartridge. The column was washed with 5 column volumes (CV) of Wash Buffer (50 mM Tris-HCl pH 8, 500 mM KCl, 1 mM TCEP) and proteins were eluted overnight with Strep Elution Buffer (50 mM Tris-HCl pH 8, 500 mM KCl, 50 mM Biotin, 1 mM TCEP). Fractions were pooled and loaded on a 5 mL HiTrap® Heparin HP affinity column equilibrated in Wash Buffer, and eluted in Heparin Elution Buffer (50 mM Tris-HCl pH 8, 1 M KCl, 1 mM TCEP). Fractions were pooled and dialyzed for 6 hrs at 4°C against Wash Buffer with addition of His-TEV protease to remove the Z-basic-TwinStrep tag. Following dialysis, the protein sample was loaded on HiLoad® 16/600 Superdex® 200 pg column equilibrated in Equilibration Buffer (25 mM HEPES/KOH pH 7.5, 200 mM KCl, 10% Glycerol, 1 mM TCEP). Eluted proteins were concentrated with 10 kDa cutoff Amicon Ultra centrifugal filters before snap-freezing in liquid nitrogen and storage at −80°C.

The open reading frame of human $HMCES^{SRAP}$ domain (amino acids 1-270) was codon-optimized for bacterial expression and cloned in pNIC in frame with a C-terminal His6-tag. $HMCES^{SRAP}$-C2S and -R98E point mutations were introduced with the Q5 site-directed mutagenesis kit (New England BioLabs), according to the manufacturer's protocols. All mutations were confirmed by Sanger sequencing. For protein expression, plasmids were transformed into BL21(DE3) *Escherichia coli* cells and grown at 37°C in Terrific broth (TB) medium until an OD of 0.7 was reached. Protein expression was induced by addition of 0.5 mM isopropyl-β-D-thiogalactoside (IPTG) for 4 hours. Cells were harvested, snap-frozen

in liquid nitrogen and stored at −80°C. Next, cells were resuspended in buffer A (50 mM HEPES/KOH pH 7.8, 500 mM KCl, 5 mM $MgCl_2$, 30 mM Imidazole, 10% Glycerol, 0.1% IGEPAL, 0.04 mg/mL Pefabloc SC, cOmplete EDTA-free protease inhibitor cocktail tablets, 1 mM Tris(2-carboxyethyl)phosphine hydrochloride (TCEP)) and lysed by sonication. All subsequent steps were carried out at 4°C. Cell lysate was incubated with smDNAse nuclease (45 U/mL lysate) for 30 min on ice prior to the removal of cell debris by centrifugation at 18,000 g for 30 min. Cleared supernatant was applied to 3 mL Ni-NTA Agarose (QIAGEN) equilibrated in buffer B (20 mM HEPES/KOH pH 7.8, 500 mM KCl, 5 mM $MgCl_2$, 30 mM Imidazole, 10% Glycerol, 1 mM TCEP). The column was washed with 15 column volumes (CV) of buffer B and proteins were eluted in 2 CV of buffer C (20 mM HEPES/KOH pH 7.8, 500 mM KCl, 5 mM $MgCl_2$, 300 mM Imidazole, 10% Glycerol, 1 mM TCEP). The sample was concentrated to 2 mL with 10 kDa cutoff Amicon Ultra centrifugal filters and further purified by size exclusion chromatography using a HiLoad® 16/600 Superdex® 200 pg column equilibrated in buffer D (20 mM HEPES/KOH pH 7.8, 150 mM KCl, 5mM $MgCl_2$, 10% Glycerol, 1 mM TCEP). Eluted proteins were concentrated with 10 kDa cutoff Am icon Ultra centrifugal filters before snap-freezing in liquid nitrogen and storage at −80°C.

The heterotrimeric human RPA protein was purified using p11d-tRPA expression plasmid (Addgene, #102613). For protein expression, the plasmid was transformed into BL21(DE3) *Escherichia coli* cells and plated on Agar plates. 1 L TB medium was inoculated with 1 colony and was left overnight at room temperature without shaking. On the next day, the cells were grown at 37°C with shaking until an OD of 0.7 was reached. Protein expression was induced by addition of 0.3 mM IPTG for 3 hours. Cells were harvested, snap-frozen in liquid nitrogen and stored at −80°C. Next, cells were resuspended in 50 mL Lysis buffer (30 mM HEPES/KOH pH 7.8, 300 mM KCl, 1 mM $MgCl_2$, 10% Glycerol, 0.02% Tween20, 0.04 mg/mL Pefabloc SC, complete EDTA-free protease inhibitor cocktail tablets, 1 mM TCEP) and lysed by sonication. Cell lysate was incubated with smDNAse nuclease (45 U/mL lysate) for 30 min on ice prior to the removal of cell debris by centrifugation at 18,000 g for 30 min. Cleared supernatant was applied to 5 mL EconoFit Affi-Gel Blue Column (BioRad), equilibrated in Buffer A1 (30 mM HEPES/KOH pH 7.8, 300 mM KCl, 10% Glycerol, 0.02% Tween20, 1 mM TCEP). The column was washed with 3 CV of Buffer A1, 3 CV of Buffer A2 (30 mM HEPES/KOH pH 7.8, 800 mM KCl, 10% Glycerol, 0.02% Tween20, 1 mM TCEP), 5 CV of Buffer A3 (30 mM HEPES/KOH pH 7.8, 500 mM NaSCN, 10% Glycerol, 0.02% Tween20, 1 mM TCEP) and 4 CV of buffer A4 (30 mM HEPES/KOH pH 7.8, 750 mM NaSCN, 10% Glycerol, 0.02% Tween20, 1 mM TCEP). Proteins were eluted with Elution Buffer (30 mM HEPES/KOH pH 7.8, 1.5 M NaSCN, 10% Glycerol, 0.02% Tween20, 1 mM TCEP). Fractions were pooled and loaded on HiLoad® 16/600 Superdex® 200 pg column equilibrated in Equilibration Buffer (20 mM HEPES/KOH pH 7.8, 300 mM KCl, 10% Glycerol, 1 mM TCEP). Eluted proteins were concentrated before snap-freezing in liquid nitrogen and storage at −80°C.

Human SPRTN WT and the catalytically inactive E112Q variant were expressed and purified as described previously [16]. The open reading frame of human Pol η was amplified by PCR using Q5® High-Fidelity DNA Polymerase (NEB #M0515) from cDNA prepared using the -Capacity cDNA Reverse Transcription Kit (ThermoFisher Scientific, #4368814)

and cloned in pNIC-Strep-Zb. Pol η was purified using the same expression and purification protocol used for production of SPRTN but using Rosetta (DE3) *Escherichia coli* cells. Pol ζ and Rev1 were purified as described [37]. The experiment shown in Figure S3D, was conducted using xlFANCJ protein kindly provided by Puck Knipscheer.

Plasmid pull-down—The plasmid pull-down assay was performed as described [38]. Briefly, streptavidin-coupled magnetic beads (Invitrogen; 10 μl per pull-down) were washed three times with 50 mM Tris (pH 7.5), 150 mM NaCl, 1 mM EDTA pH 8, 0.02% Tween-20. Biotinylated LacI was added to the beads (4 pmol per 10 μl beads) and incubated at room temperature for 40 min. The beads were then washed four times with Pull-down Buffer (10 mM HEPES (pH 7.7), 50 mM KCl, 2.5 mM $MgCl_2$, 250 mM sucrose, 0.25 mg/ml BSA, 0.02% Tween-20) and resuspended in 40 μl of the same buffer. The bead suspension was stored on ice until needed. At the indicated times, 4.0 μl samples of the replication reaction were withdrawn and gently mixed with LacI-coated streptavidin Dynabeads. The suspension was immediately placed on a rotating wheel and incubated for 30 min at 4 °C. The beads and associated proteins were isolated by centrifugation through a sucrose cushion (10 mM HEPES pH 7.7, 2.5 mM $MgCl_2$, 50 mM KCl, 0.5 M sucrose, 0.02 % Tween), then washed once with Pull-down Buffer. All residual buffer was removed, and the beads were resuspended in 20 μl of 2X Laemmli sample buffer. Equal volumes of the protein samples were blotted with the indicated antibodies.

DPC pull-down—The DPC pull-down assay to quantify the amount M.HpaII was removed from the plasmid during DPC repair was performed as previously described [6]. Briefly, streptavidin-coupled magnetic beads (Invitrogen; 10 μl per pull-down) were washed three times with 50 mM Tris (pH 7.5), 150 mM NaCl, 1 mM EDTA pH 8, 0.02% Tween-20. Biotinylated LacI was added to the beads (4 pmol per 10 μl beads) and incubated at room temperature for 40 min. The beads were then washed four times with Wash Buffer (20 mM HEPES (pH 7.5), 150 mM NaCl, 2 mM EDTA, 0.5% NP-40) and resuspended in 10 μ/sample of the same buffer. The bead suspension was stored on ice until needed. At the indicated times, 4.5 μl samples of the replication reaction were withdrawn and mixed in 300 μl of Wash Buffer. After the last timepoint 10 μl of lacI coated streptavidin beads were added to each sample. The suspension was immediately placed on a rotating wheel and incubated for 30 min at 4 °C. Following the incubation the beads were then washed three times with 500 μl of Pull-down Buffer on a magnet. Following washes the beads were washed three times with Benzonase buffer (20 mM Tris pH 7.5, 150 mM NaCl, 2 mM $MgCl_2$, 0.02 % Tween 20). Where indicated samples were then split and half the sample was treated with the deubiquitylating enzyme Usp21 for 1 hour at 37 °C. Subsequently, all residual buffer was removed, and the beads were resuspended in 7.5 μl of Benzonase buffer containing 1 μl of Benzonase (Sigma) at 37 °C for 1 hour to allow for DNA digestion and DPC elution, after which the beads were pelleted and the supernatant M.HpaII eluate was mixed with 2X Laemmli sample buffer for subsequent western blotting analysis. Equal volumes of the protein samples were blotted with the indicated antibodies. To help visualize bands in plasmid and DPC pull-down experiments, brightness and contrast of some Western blots were adjusted globally using ImageJ. Quantification was performed using ImageJ.

Generation of HMCES^{SRAP}-DPCs—DPCs were generated between HMCES^{SRAP} WT and mutant variants and a 30mer Cy5-fluorescently-labelled forward oligonucleotide oDY_54. HMCES^{SRAP} was prediluted to 40 μM in purification buffer D and forward oligonucleotide was prediluted to 1 μM in DNA dilution buffer (50 mM HEPES/KOH pH 7.5, 100 mM KCl, 10% Glycerol, 0.4 mg/mL BSA). Cross-linking was carried out in 10 μL final volume containing 1 μL forward oligonucleotide, 0.5 μL HMCES^{SRAP}, 0.48 μL UDG (New England BioLabs) and 8.02 μL reaction buffer (20 mM HEPES/KOH pH 7.5, 50 mM KCl, 10 mM $MgCl_2$, 2 mM TCEP, 0.1 mg/ml BSA), resulting in final concentrations of 0.1 μM DNA, 2 μM HMCES^{SRAP}, and 0.1 U/μl UDG. The reaction was incubated for 1 hour at 37°C. Next, 1 μL of 15mer complementary reverse oligonucleotide oHR_127 (12 μM in nuclease-free H_2O) was added to the cross-linking reaction. Annealing was performed by incubating the reaction for 2 min at 37°C followed by a decrease in temperature of 1°C/min until 20°C was reached. In experiments using ssDNA DPCs, the reverse oligonucleotide was replaced by H_2O. In experiments using heat-denatured DPCs, the reactions were incubated for 5 minutes at 60°C prior to reverse oligonucleotide annealing. All DPCs were prepared immediately prior to cleavage assays.

For analysis of DPCs by native PAGE, HMCES^{SRAP} was prediluted to 40 μM in purification buffer D and forward oligonucleotide was prediluted to 1 μM in DNA dilution buffer. The assay was carried out in 10 μL final volume with 1 μL forward oligonucleotide, 0.5 μL HMCES^{SRAP}, 0.48 μL UDG (1 U) and 8.02 μL reaction buffer (20 mM HEPES/KOH pH 7.5, 50 mM KCl, 10 mM $MgCl_2$, 2 mM TCEP, 0.1 mg/ml BSA). The reactions were incubated for 1 hour at 37°C to allow DPC formation. For heat-denaturation, DPCs were then incubated for 5 minutes at 60°C. 4 μL of 6x Orange G loading dye was added and the samples were separated on 6% native PAGE gels with 0.5x TBE as running buffer at room temperature. Gels were photographed using a BioRad Chemidoc MP system using appropriate filter settings for Cy5 fluorescence. To help visualize bands, brightness and contrast of some gel images were adjusted globally using ImageJ. Quantification was performed using ImageJ; the fraction of DPC in the well was determined by dividing the amount of DPC retained in the well by the total amount of DPCs (retained in well plus DPC in gel).

Generation of protein G-DPCs—Recombinant N-terminally His-tagged protein G (BioVision, #6510) was conjugated to a fluorescently-labelled oligonucleotide 30_FAM_X15 using proFIRE Amine Coupling Kit (Dynamic Biosensors, #PF-NH2-1) as described previously [39].

DPC cleavage assays—For the experiment shown in Figure 3A, FANCJ dependent-cleavage of HMCES^{SRAP}-DPCs by SPRTN was assessed in a reaction volume of 10 μL containing 1 μL of the HMCES^{SRAP} DNA cross-linking reaction described above, 80 nM FANCJ, 100 nM SPRTN in a final reaction buffer of 9.5 mM HEPES/KOH pH 7.5, 70 mM KCl, 2 mM $MgCl_2$, 2 mM ATP, 2 % Glycerol, 5.5 mM TCEP and 0.1 mg/ml BSA. For the experiments shown in Figure 4A, S3B, and S3E, the reaction was performed identically, but using 100 nM FANCJ in a final reaction buffer of 17 mM HEPES/KOH pH 7.5, 85 mM KCl, 2 mM $MgCl_2$, 2 mM ATP, 3 % Glycerol, 5.5 mM TCEP and 0.1 mg/ml BSA.

For the experiment shown in Figure S3D, the reaction was performed identical, but using 20 nM *X.l.* rFANCJ in a final reaction buffer of 12 mM HEPES/KOH pH 7.5, 2 mM Tris/HCl, 20 mM NaCl, 70 mM KCl, 2 mM $MgCl_2$, 2 mM ATP, 2 % Glycerol, 5.5 mM TCEP and 0.1 mg/ml BSA. Reactions were incubated for 1 hour at 30°C and stopped by the addition of 5.5 μL SDS loading buffer. The reactions were then boiled for 1 minute at 95°C and resolved on 4-12% or 12% SDS-PAGE gels. Gels were photographed using a BioRad Chemidoc MP system using appropriate filter settings for Cy5 fluorescence. ImageJ was used for quantification; the fraction of cleaved DPCs was determined by dividing the amount of cleaved DPCs by the total amount of DPCs (cleaved plus uncleaved).

DNA binding assays—Electrophoretic mobility shift assays (EMSAs) were used to analyze binding of recombinant $HMCES^{SRAP}$ WT and mutant variants to a Cy5-fluorescently labelled 30-mer oligonucleotide oDY_54. $HMCES^{SRAP}$ was prediluted to 40, 10 and 2.5 μM in purification buffer D and forward oligonucleotide was prediluted to 1 μM in DNA dilution buffer. Binding was carried out in 10 μL final volume with 1 μL forward oligonucleotide, 0.5 μL $HMCES^{SRAP}$ and 8.5 μL reaction buffer (20 mM HEPES/KOH pH 7.5, 50 mM KCl, 10 mM $MgCl_2$, 2 mM TCEP, 0.1 mg/ml BSA). The reactions were incubated for 20 min on ice. 4 μL of 6x Orange G loading dye was added and the samples were separated on 6% native PAGE gels with 0.5x TBE as running buffer at 4°C. Gels were photographed using a BioRad Chemidoc MP system using appropriate filter settings for Cy5 fluorescence.

Limited proteolysis—Limited proteolysis was used to analyze FANCJ-dependent $HMCES^{SRAP}$-DPC unfolding. For Figure 4B, FANCJ dependent $HMCES^{SRAP}$-DPC unfolding was assessed in a reaction volume of 10 μL containing 1 μL of the $HMCES^{SRAP}$ DNA cross-linking reaction using a single-stranded oligonucleotide oDY_54, 100 nM FANCJ, 2 ng Trypsin Gold (Promega) in a final reaction buffer of 22 mM HEPES/KOH pH 7.5, 85 mM KCl, 2 mM $MgCl_2$, 2 mM ATP, 3 % Glycerol, 5.5 mM TCEP and 0.1 mg/ml BSA. Limited proteolysis of protein G-DPCs was performed identically using 10 nM of purified protein G-oligonucleotide conjugate as substrate. For Figure S5C, limited proteolysis of $HMCES^{SRAP}$-DPCs was performed identical, but using 80 nM FANCJ in a final reaction buffer of 22 mM HEPES/KOH pH 7.5, 60 mM KCl, 2 mM $MgCl_2$, 2 mM ATP, 2 % Glycerol, 5.5 mM TCEP and 0.1 mg/ml BSA. Reactions were incubated for 5, 10 or 15 min at 30°C and stopped by the addition of 5.5 μL SDS loading buffer. The reactions were then boiled for 1 minute at 95°C and resolved on 4-12% SDS-PAGE gels. Gels were photographed using a BioRad Chemidoc MP system using appropriate filter settings for Cy5 or 6-FAM fluorescence.

DNA footprinting—Restriction site cleavage was used to analyze DNA accessibility in proximity to a $HMCES^{SRAP}$-DPC. $HMCES^{SRAP}$ DNA cross-linking reactions were performed as described above. For Figure 5A left panel and S5A, a Cy5-fluorescently-labelled forward oligonucleotide oMD129 and oMD132 reverse oligonucleotide were used. For Figure 5A right panel, a Cy5-fluorescently-labelled forward oligonucleotide oMD137 and oMD138 reverse oligonucleotide were used. For Figure 5B, a Cy5-fluorescently-labelled forward oligonucleotide oDY116 and oDY117 reverse oligonucleotide were used.

The reaction volume of 10 μL contained 1 μL of the HMCES^{SRAP} DNA cross-linking reaction, 100 nM FANCJ, 100 nM SPRTN, 0.05 U HaeIII (New England BioLabs) in a final reaction buffer of 17 mM HEPES/KOH pH 7.5, 85 mM KCl, 2 mM $MgCl_2$, 2 mM ATP, 3 % Glycerol, 5.5 mM TCEP and 0.1 mg/ml BSA. Reactions were incubated for 1 hour at 37°C and stopped by the addition of 5.5 μL SDS loading buffer. The reactions were then boiled for 1 minute at 95°C and resolved on 4-12% or 12% SDS-PAGE gels. Gels were photographed using a BioRad Chemidoc MP system using appropriate filter settings for Cy5 fluorescence. To help visualize bands, brightness and contrast of some gel images were adjusted globally using ImageJ. Quantification was performed using ImageJ; the fraction of HaeIII-cut DPC was determined by dividing the amount of HaeIII-cut DPCs by the total amount of DPCs (cut plus uncut).

Primer extension—Primer extension assays were used to analyze FANCJ-dependent HMCES^{SRAP}-DPC bypass by TLS Polymerases Pol ζ-Rev1 and Pol η. HMCES^{SRAP} DNA cross-linking reactions were performed as described above, but forward oDY109 and reverse oDY98 oligonucleotides were annealed prior to DPC formation. FANCJ dependent primer extension with Pol ζ-Rev1 was assessed in a reaction volume of 10 μL containing 1 μL of the HMCES^{SRAP} DNA cross-linking reaction, 80 nM FANCJ, 25 nM Pol ζ, 40 nM Rev1 in a final reaction buffer of 17 mM HEPES/KOH pH 7.5, 60 mM KCl, 20 mM NaCl, 4 % Glycerol, 5.5 mM TCEP, 2 mM ATP, 0.2 mM (each) dNTPs, 2 mM $MgCl_2$, 0.1 mg/ml BSA. FANCJ dependent primer extension with Pol η was performed identical, but using 5 nM Pol η in a final reaction buffer of 17 mM HEPES/KOH pH 7.5, 75 mM KCl, 4 % Glycerol, 5.5 mM TCEP, 2 mM ATP, 0.2 mM (each) dNTPs, 2 mM $MgCl_2$, 0.1 mg/ml BSA. Reactions were incubated for 30 min at 37°C and stopped by the addition of 10 μL UREA loading buffer (8M UREA, 15% Ficoll). The reactions were then boiled for 10 minutes at 95°C and resolved on denaturing 12% UREA-PAGE gels (12% Acrylamide, 8M UREA, 1xTBE) at 60°C in 1xTBE running buffer. Gels were photographed using a BioRad Chemidoc MP system using appropriate filter settings for 6-FAM fluorescence.

Generation of cell lines—To generate U20S T-Rex Flp-In *FANCJ* KO and *AAVS1* control clones, gRNA FANCJ_2 and gRNA_AAVS1 were cloned into pX330-Puro (Addgene #82580). gRNA plasmids were then transiently transfected using Lipofectamine 2000 (Invitrogen) according to the manufacturer's instructions. 16 h after transfection, cells were selected in puromycin (1 μg/ml)-containing DMEM media for 3 days. For single clone generation, puromycin-selected cells were reseeded in 96-well plates (0.75 cell/well). Single clones were expanded and analyzed by western blotting using anti-FANCJ antibody (Novus Biologicals #NBP1-31883) and anti-Actin antibody (Santa Cruz, sc-47778).

For doxycycline-includible complementation of *FANCJ* KO cells, coding sequences of FANCJ-WT and FANCJ-K52R (Addgene, #17642 and #17643, respectively) were amplified using Q5 Master Mix (M0544, NEB) and primers oPW_632 and oPW_633 before being shuttled into p221 plasmid using BP clonase (Thermo Fischer). Next, *FANCJ* sequences were subcloned into pcDNA5/FRT/TO-Venus-3xFlag-Gateway (Addgene, #40999) using LR clonase, before generation of stable cell lines using the T-REx Flp-In system (Thermo Fisher) according to manufacturer's instructions. Briefly, cells were grown

to 50% confluency in six-well plates prior to transfection of pOG44 (1.8 μg) and the respective pcDNA5-FRT/TO plasmids (0.2 μg, containing FANCJ-Venus-3xFlag, FANCJ-K52R-Venus-3xFlag, FANCJ-A349P-Venus-3xFlag (generated using site-directed mutagenesis using primers oPW_673 and oPW_674), or Venus-3xFlag (the gateway recombination cassette was deleted using oPW_570 and oPW_571) using Lipofectamine 2000 (Invitrogen). 16h after transfection, cells were selected in 150 μg/ml Hygromycin B (Fisher Scientific)-containing DMEM media for 10 days.

Formaldehyde sensitivity—To measure formaldehyde sensitivity of U2OS T-REx Flp-In *AAVS1* #2, #3 and *FANCJ* KO #2, #8, #10 clones, were counted and seeded in 12-well plates (1000 cells per well). The next day, cells were treated with media containing 0, 12.5, 25, or 50 μM formaldehyde in technical triplicates. After 7 days, cell viability was assessed by AlamarBlue assay (Sigma, R7017-1G, 1 % in PBS). Formaldehyde sensitivity of complemented U2OS T-REx Flp-In *FANCJ* KO #8 cells was determined as described above but using media containing doxycycline (1 μg/ml) to induce protein expression.

QUANTIFICATION AND STATISTICAL ANALYSIS

Statistical details of each experiment (including the exact value of n, what n represents and precision measures) can be found in the figure legends.

Supplementary Material

Refer to Web version on PubMed Central for supplementary material.

Acknowledgements

We thank Daniel Semlow and Alex Wu for critical feedback on the manuscript, Kim Remans and Julia Flock (EMBL Protein Expression and Purification Core Facility) for help with protein production, and Puck Knipscheer and F. Ulrich Hartl for providing antibodies and/or recombinant proteins. We thank Alex Wu for performing one of the repeats of Figure 2A, Olga Kochenova for help in preparing the revision, and Sophie Dürauer for preparation of protein G-DPCs. This work was supported by NIH grant HL098316 to J.C.W. J.C.W. is an investigator of the Howard Hughes Medical Institute and an American Cancer Society Research Professor. Research in the lab of J.S. is supported by the European Research Council under the European Union's Horizon 2020 research and innovation program (grant agreement number 801750), by the Alfried Krupp Prize for Young University Teachers awarded by the Alfried Krupp von Bohlen und Halbach Foundation, the European Molecular Biology Organization (YIP4644), the Vallee Foundation, and by the Deutsche Forschungsgemeinschaft (DFG, German Research Foundation) (Project ID 213249687 – SFB 1064). NIH grant GM118129 to Peter M. Burgers supported R.B-B.

References

1. Cortez D (2019). Replication-Coupled DNA Repair. Mol Cell 74, 866–876. 10.1016/j.molcel.2019.04.027. [PubMed: 31173722]
2. Berti M, Cortez D, and Lopes M (2020). The plasticity of DNA replication forks in response to clinically relevant genotoxic stress. Nat Rev Mol Cell Biol 21, 633–651. 10.1038/s41580-020-0257-5. [PubMed: 32612242]
3. Weickert P, and Stingele J (2022). DNA-Protein Crosslinks and Their Resolution. Annu Rev Biochem 91, 157–181. 10.1146/annurev-biochem-032620-105820. [PubMed: 35303790]
4. Stingele J, Schwarz MS, Bloemeke N, Wolf PG, and Jentsch S (2014). A DNA-dependent protease involved in DNA-protein crosslink repair. Cell 158, 327–338. 10.1016/j.cell.2014.04.053. [PubMed: 24998930]

5. Duxin JP, Dewar JM, Yardimci H, and Walter JC (2014). Repair of a DNA-protein crosslink by replication-coupled proteolysis. Cell 159, 346–357. 10.1016/j.cell.2014.09.024. [PubMed: 25303529]
6. Larsen NB, Gao AO, Sparks JL, Gallina I, Wu RA, Mann M, Raschle M, Walter JC, and Duxin JP (2019). Replication-Coupled DNA-Protein Crosslink Repair by SPRTN and the Proteasome in Xenopus Egg Extracts. Mol Cell 73, 574–588 e577. 10.1016/j.molcel.2018.11.024. [PubMed: 30595436]
7. Vaz B, Popovic M, Newman JA, Fielden J, Aitkenhead H, Halder S, Singh AN, Vendrell I, Fischer R, Torrecilla I, et al. (2016). Metalloprotease SPRTN/DVC1 Orchestrates Replication-Coupled DNA-Protein Crosslink Repair. Mol Cell 64, 704–719. 10.1016/j.molcel.2016.09.032. [PubMed: 27871366]
8. Stingele J, Bellelli R, Alte F, Hewitt G, Sarek G, Maslen SL, Tsutakawa SE, Borg A, Kjaer S, Tainer JA, et al. (2016). Mechanism and Regulation of DNA-Protein Crosslink Repair by the DNA-Dependent Metalloprotease SPRTN. Mol Cell 64, 688–703. 10.1016/j.molcel.2016.09.031. [PubMed: 27871365]
9. Maskey RS, Flatten KS, Sieben CJ, Peterson KL, Baker DJ, Nam HJ, Kim MS, Smyrk TC, Kojima Y, Machida Y, et al. (2017). Spartan deficiency causes accumulation of Topoisomerase 1 cleavage complexes and tumorigenesis. Nucleic Acids Res 45, 4564–4576. 10.1093/nar/gkx107. [PubMed: 28199696]
10. Morocz M, Zsigmond E, Toth R, Enyedi MZ, Pinter L, and Haracska L (2017). DNA-dependent protease activity of human Spartan facilitates replication of DNA-protein crosslink-containing DNA. Nucleic Acids Res 45, 3172–3188. 10.1093/nar/gkw1315. [PubMed: 28053116]
11. Lopez-Mosqueda J, Maddi K, Prgomet S, Kalayil S, Marinovic-Terzic I, Terzic J, and Dikic I (2016). SPRTN is a mammalian DNA-binding metalloprotease that resolves DNA-protein crosslinks. Elife 5. 10.7554/eLife.21491.
12. Lessel D, Vaz B, Halder S, Lockhart PJ, Marinovic-Terzic I, Lopez-Mosqueda J, Philipp M, Sim JC, Smith KR, Oehler J, et al. (2014). Mutations in SPRTN cause early onset hepatocellular carcinoma, genomic instability and progeroid features. Nat Genet 46, 1239–1244. 10.1038/ng.3103. [PubMed: 25261934]
13. Maskey RS, Kim MS, Baker DJ, Childs B, Malureanu LA, Jeganathan KB, Machida Y, van Deursen JM, and Machida YJ (2014). Spartan deficiency causes genomic instability and progeroid phenotypes. Nat Commun 5, 5744. 10.1038/ncomms6744. [PubMed: 25501849]
14. Sparks JL, Chistol G, Gao AO, Raschle M, Larsen NB, Mann M, Duxin JP, and Walter JC (2019). The CMG Helicase Bypasses DNA-Protein Cross-Links to Facilitate Their Repair. Cell 176, 167–181 e121. 10.1016/j.cell.2018.10.053. [PubMed: 30595447]
15. Gallina I, Hendriks IA, Hoffmann S, Larsen NB, Johansen J, Colding-Christensen CS, Schubert L, Selles-Baiget S, Fabian Z, Kuhbacher U, et al. (2021). The ubiquitin ligase RFWD3 is required for translesion DNA synthesis. Mol Cell 81, 442–458 e449. 10.1016/j.molcel.2020.11.029. [PubMed: 33321094]
16. Reinking HK, Kang HS, Gotz MJ, Li HY, Kieser A, Zhao S, Acampora AC, Weickert P, Fessler E, Jae LT, et al. (2020). DNA Structure-Specific Cleavage of DNA-Protein Crosslinks by the SPRTN Protease. Mol Cell 80, 102–113 e106. 10.1016/j.molcel.2020.08.003. [PubMed: 32853547]
17. Olivieri M, Cho T, Alvarez-Quilon A, Li K, Schellenberg MJ, Zimmermann M, Hustedt N, Rossi SE, Adam S, Melo H, et al. (2020). A Genetic Map of the Response to DNA Damage in Human Cells. Cell. 10.1016/j.cell.2020.05.040.
18. Barber LJ, Youds JL, Ward JD, McIlwraith MJ, O'Neil NJ, Petalcorin MI, Martin JS, Collis SJ, Cantor SB, Auclair M, et al. (2008). RTEL1 maintains genomic stability by suppressing homologous recombination. Cell 135, 261–271. 10.1016/j.cell.2008.08.016. [PubMed: 18957201]
19. Brosh RM Jr., and Cantor SB (2014). Molecular and cellular functions of the FANCJ DNA helicase defective in cancer and in Fanconi anemia. Front Genet 5, 372. 10.3389/fgene.2014.00372. [PubMed: 25374583]
20. Sato K, Martin-Pintado N, Post H, Altelaar M, and Knipscheer P (2021). Multistep mechanism of G-quadruplex resolution during DNA replication. Sci Adv 7, eabf8653. 10.1126/sciadv.abf8653. [PubMed: 34559566]

21. Matsuzaki K, Borel V, Adelman CA, Schindler D, and Boulton SJ (2015). FANCJ suppresses microsatellite instability and lymphomagenesis independent of the Fanconi anemia pathway. Genes Dev 29, 2532–2546. 10.1101/gad.272740.115. [PubMed: 26637282]
22. Sommers JA, Banerjee T, Hinds T, Wan B, Wold MS, Lei M, and Brosh RM Jr. (2014). Novel function of the Fanconi anemia group J or RECQ1 helicase to disrupt protein-DNA complexes in a replication protein A-stimulated manner. J Biol Chem 289, 19928–19941. 10.1074/jbc.M113.542456. [PubMed: 24895130]
23. Mohni KN, Wessel SR, Zhao R, Wojciechowski AC, Luzwick JW, Layden H, Eichman BF, Thompson PS, Mehta KPM, and Cortez D (2019). HMCES Maintains Genome Integrity by Shielding Abasic Sites in Single-Strand DNA. Cell 176, 144–153 e113. 10.1016/j.cell.2018.10.055. [PubMed: 30554877]
24. Semlow DR, MacKrell VA, and Walter JC (2022). The HMCES DNA-protein cross-link functions as an intermediate in DNA interstrand cross-link repair. Nat Struct Mol Biol. 10.1038/s41594-022-00764-0.
25. Tretyakova NY, Groehler A.t., and Ji S (2015). DNA-Protein Cross-Links: Formation, Structural Identities, and Biological Outcomes. Acc Chem Res 48, 1631–1644. 10.1021/acs.accounts.5b00056. [PubMed: 26032357]
26. Halabelian L, Ravichandran M, Li Y, Zeng H, Rao A, Aravind L, and Arrowsmith CH (2019). Structural basis of HMCES interactions with abasic DNA and multivalent substrate recognition. Nat Struct Mol Biol 26, 607–612. 10.1038/s41594-019-0246-6. [PubMed: 31235913]
27. Thompson PS, Amidon KM, Mohni KN, Cortez D, and Eichman BF (2019). Protection of abasic sites during DNA replication by a stable thiazolidine protein-DNA cross-link. Nat Struct Mol Biol 26, 613–618. 10.1038/s41594-019-0255-5. [PubMed: 31235915]
28. Wu Y, Sommers JA, Suhasini AN, Leonard T, Deakyne JS, Mazin AV, Shin-Ya K, Kitao H, and Brosh RM Jr. (2010). Fanconi anemia group J mutation abolishes its DNA repair function by uncoupling DNA translocation from helicase activity or disruption of protein-DNA complexes. Blood 116, 3780–3791. 10.1182/blood-2009-11-256016. [PubMed: 20639400]
29. Klimasauskas S, Kumar S, Roberts RJ, and Cheng X (1994). HhaI methyltransferase flips its target base out of the DNA helix. Cell 76, 357–369. [PubMed: 8293469]
30. Li F, Raczynska JE, Chen Z, and Yu H (2019). Structural Insight into DNA-Dependent Activation of Human Metalloprotease Spartan. Cell Rep 26, 3336–3346 e3334. 10.1016/j.celrep.2019.02.082. [PubMed: 30893605]
31. Vannier JB, Sarek G, and Boulton SJ (2014). RTEL1: functions of a disease-associated helicase. Trends Cell Biol 24, 416–425. 10.1016/j.tcb.2014.01.004. [PubMed: 24582487]
32. Bharti SK, Awate S, Banerjee T, and Brosh RM (2016). Getting Ready for the Dance: FANCJ Irons Out DNA Wrinkles. Genes (Basel) 7. 10.3390/genes7070031.
33. Walter J, Sun L, and Newport J (1998). Regulated chromosomal DNA replication in the absence of a nucleus. Mol Cell 1, 519–529. [PubMed: 9660936]
34. Sparks J, and Walter JC (2018). Extracts for Analysis of DNA Replication in a Nucleus-Free System. Cold Spring Harb Protoc. 10.1101/pdb.prot097154.
35. Castillo Bosch P, Segura-Bayona S, Koole W, van Heteren JT, Dewar JM, Tijsterman M, and Knipscheer P (2014). FANCJ promotes DNA synthesis through G-quadruplex structures. EMBO J 33, 2521–2533. 10.15252/embj.201488663. [PubMed: 25193968]
36. Walter J, and Newport J (2000). Initiation of eukaryotic DNA replication: origin unwinding and sequential chromatin association of Cdc45, RPA, and DNA polymerase alpha. Mol Cell 5, 617–627. [PubMed: 10882098]
37. Kochenova OV, Bezalel-Buch R, Tran P, Makarova AV, Chabes A, Burgers PM, and Shcherbakova PV (2017). Yeast DNA polymerase zeta maintains consistent activity and mutagenicity across a wide range of physiological dNTP concentrations. Nucleic Acids Res 45, 1200–1218. 10.1093/nar/gkw1149. [PubMed: 28180291]
38. Budzowska M, Graham TG, Sobeck A, Waga S, and Walter JC (2015). Regulation of the Rev1-pol zeta complex during bypass of a DNA interstrand cross-link. EMBO J 34, 1971–1985. 10.15252/embj.201490878. [PubMed: 26071591]

39. Reinking HK, and Stingele J (2021). Protein-oligonucleotide conjugates as model substrates for DNA-protein crosslink repair proteases. STAR Protoc 2, 100591. 10.1016/j.xpro.2021.100591. [PubMed: 34189469]

40. Semlow DR, MacKrell VA, and Walter JC (2022). The HMCES DNA-protein cross-link functions as an intermediate in DNA interstrand cross-link repair. Nat Struct Mol Biol 29, 451–462. 10.1038/s41594-022-00764-0. [PubMed: 35534579]

41. McGarry TJ, and Kirschner MW (1998). Geminin, an inhibitor of DNA replication, is degraded during mitosis. Cell 93, 1043–1053. [PubMed: 9635433]

42. Dewar JM, Low E, Mann M, Raschle M, and Walter JC (2017). CRL2(Lrr1) promotes unloading of the vertebrate replisome from chromatin during replication termination. Genes Dev 31, 275–290. 10.1101/gad.291799.116. [PubMed: 28235849]

43. Dewar JM, Budzowska M, and Walter JC (2015). The mechanism of DNA replication termination in vertebrates. Nature 525, 345–350. 10.1038/nature14887. [PubMed: 26322582]

Highlights

- FANCJ unfolds DNA-protein cross-links (DPCs)
- FANCJ is required for SPRTN-mediated DPC proteolysis during replication
- FANCJ is essential for translesion DNA synthesis past intact DPCs
- FANCJ promotes bypass of covalent and non-covalent protein barriers

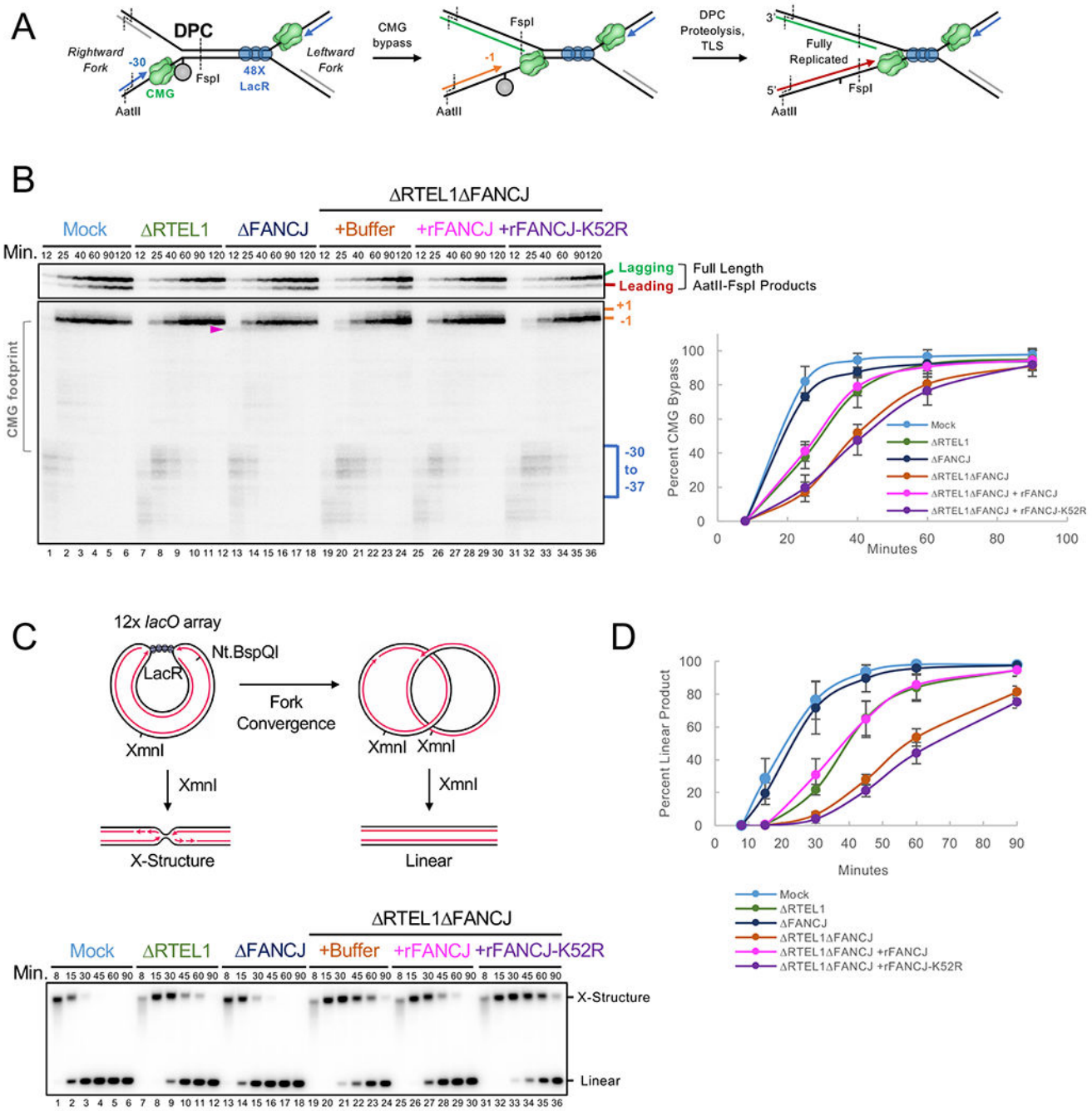

Figure 1. FANCJ supports CMG bypass of covalent and non-covalent nucleoprotein complexes in the absence of RTEL1

(A) Schematic of nascent strand products released by AatII and FspI digestion of pDPC^{Lead}. **(B)** pDPC^{Lead} was pre-bound with LacR to prevent the leftward replication fork from reaching the DPC and replicated in the indicated egg extracts containing ^{32}P[α]-dATP and supplemented with buffer, recombinant wildtype FANCJ, or ATPase mutant FANCJ-K52R, as indicated. At different times, DNA was extracted and digested with AatII and FspI, separated on a denaturing polyacrylamide gel, and visualized by autoradiography. The lower

autoradiogram shows nascent leading strands generated by the rightward replication fork, and the upper autoradiogram shows leading and lagging extension products. Light blue bracket, CMG footprint (−30 to −37); orange bracket, products stalled at the adducted base (−1 to +1). The percentage of leading strands that approached from the −30 cluster to the −1 cluster was quantified, and the mean of n = 3 experiments is graphed. Error bars represent the SD. **(C)** Top: DNA structures generated by XmnI cleavage of $pLacO_{12}$ before and after forks progress through the LacR array. $pLacO_{12}$ was pre-incubated with LacR and replicated in the indicated egg extracts containing [α–^{32}P]-dATP. DNA was recovered, digested with XmnI, resolved by native agarose gel electrophoresis, and visualized by autoradiography. **(D)** Quantification of the rate of linear product formation in the experiment shown in Panel (C). See also Figure S1.

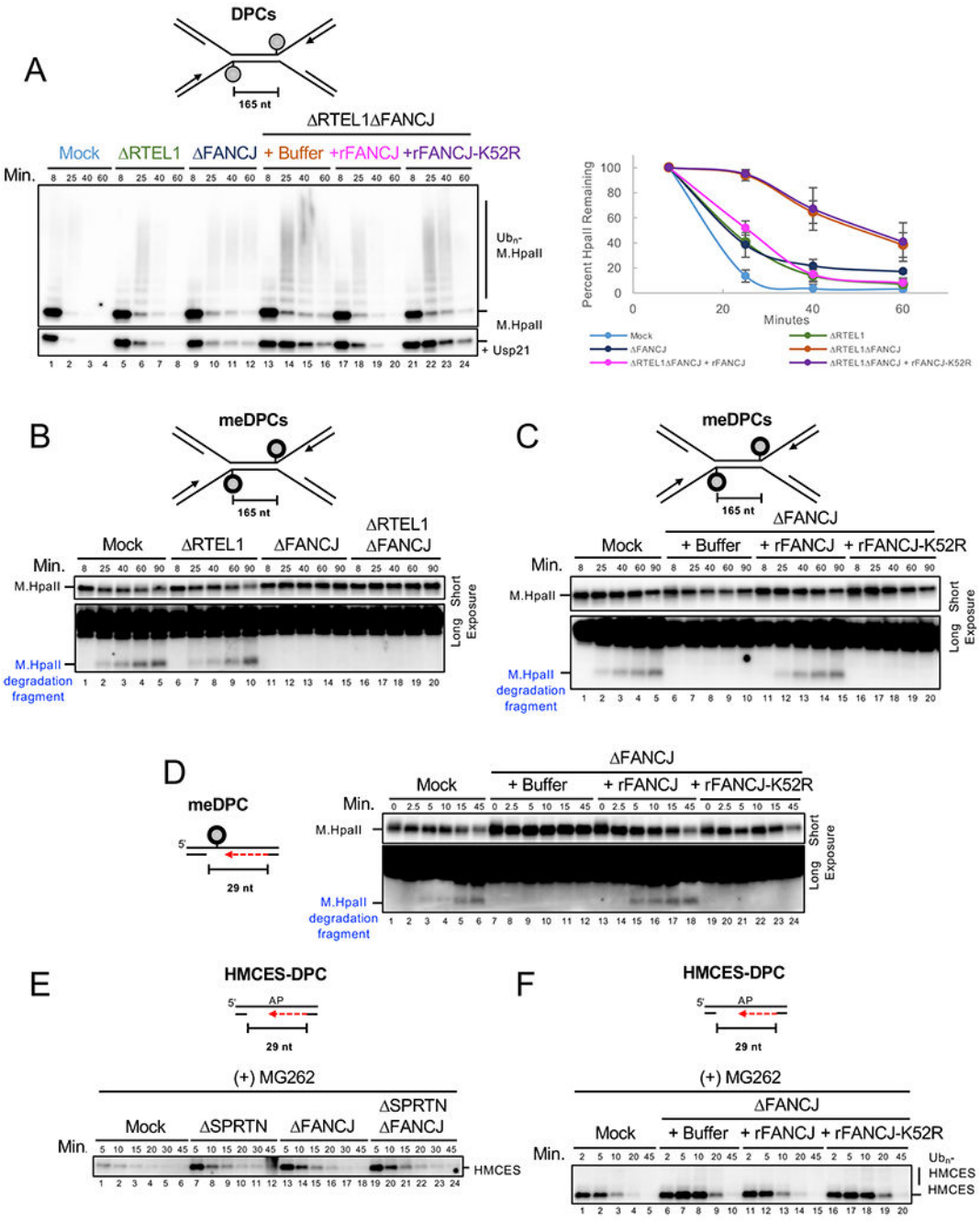

Figure 2. FANCJ is required for DPC proteolysis

(A) pDPC2x^{Lead} was replicated in the indicated egg extracts supplemented with buffer, recombinant wildtype FANCJ, or ATPase mutant FANCJ-K52R. At the indicated times, plasmid was recovered under stringent conditions, the samples were split and either mock treated (upper panel) or treated with the de-ubiquitylating enzyme Usp21 (lower panel), followed by DNA digestion and blotting for HpaII. Signal from the Usp21-treated sample was quantified, and peak signal was assigned a value of 100%. The mean of n = 3 independent experiments is graphed. Error bars represent SD. **(B)** pmeDPC2x^{Lead} was

replicated in the indicated egg extracts. At the indicated times, plasmid was recovered under stringent conditions, followed by DNA digestion, and the resulting samples were blotted for HpaII. **(C)** pmeDPC2x^{Lead} was replicated in the indicated egg extracts supplemented with buffer, recombinant wildtype FANCJ, or ATPase mutant FANCJ-K52R and HpaII was analyzed as in (A). **(D)** pmeDPC^{ssDNA} was incubated directly in the indicated nucleoplasmic egg extract (NPE) supplemented with buffer, recombinant wildtype FANCJ, or ATPase mutant FANCJ-K52R without prior licensing in HSS to prevent replication initiation [33]. Plasmid was isolated and blotted for HpaII as in (A). **(E)** pAP^{ssDNA} was incubated in the indicated NPE which caused HMCES cross-linking to the AP site. Plasmid was isolated by the stringent pull-down procedure as in (A) but the resulting samples were blotted for HMCES instead of HpaII. **(F)** pAP^{ssDNA} was incubated in the indicated NPE supplemented with MG262 and buffer, recombinant wildtype FANCJ, or ATPase mutant FANCJ-K52R without prior licensing in HSS. Plasmid was isolated and analyzed as in (E). See also Figure S2.

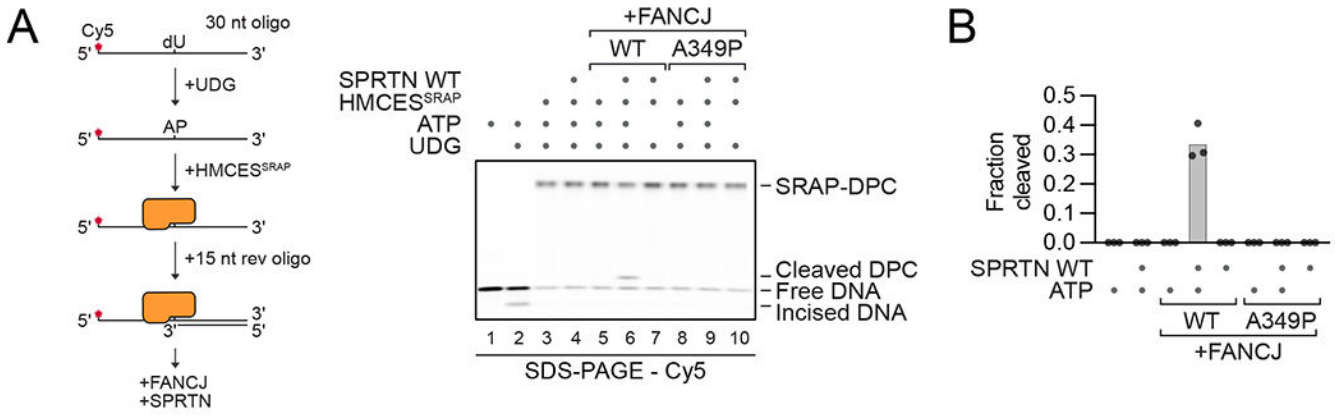

Figure 3. FANCJ is sufficient to promote SPRTN proteolysis of a native DPC

(A) Schematic of the generation of HMCES^{SRAP}-DPCs (left panel). Free DNA or the human HMCES^{SRAP}-DPC were incubated alone or in the presence of recombinant human FANCJ (WT or A349P), human SPRTN, and ATP as indicated for 1 h at 30°C prior to separation by denaturing SDS-PAGE (right panel). **(B)** Quantification of the DPC cleavage assay shown in (A). Bar graph shows the mean of three independent experiments. See also Figure S3.

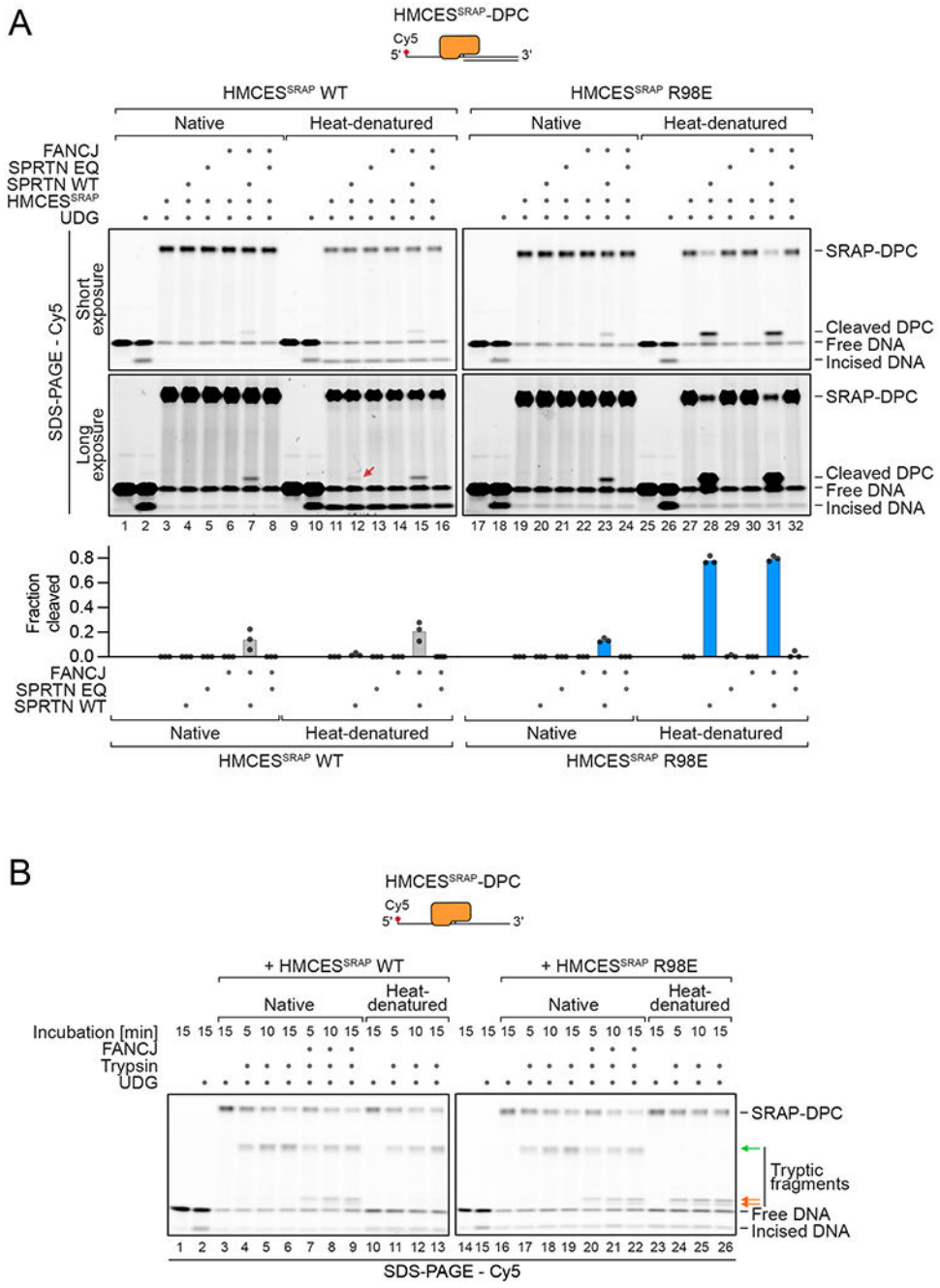

Figure 4. FANCJ unfolds the DPC

(A) Cleavage of native or heat-denatured HMCES^{SRAP}-DPCs (WT or the DNA-binding-deficient variant R98E) by SPRTN. Free DNA or HMCES^{SRAP}-DPCs were incubated alone or in the presence of recombinant FANCJ and SPRTN (WT or the catalytically inactive E112Q (EQ) variant) for 1 h at 30°C prior to separation by denaturing SDS-PAGE (upper panel). Quantification of the DPC cleavage assay: bar graph represents the mean of three independent experiments (lower panel). **(B)** Limited proteolysis of HMCES^{SRAP}-DPCs. Free DNA or the human HMCES^{SRAP}-DPC (WT or R98E) were incubated alone or in the

presence of recombinant human FANCJ and trypsin as indicated for 5, 10 or 15 min at 30°C prior to analysis by denaturing SDS-PAGE. Green arrow, tryptic cleavage site accessible in natively folded HMCES^{SRAP}-DPC; Orange arrows, cleavage sites exposed upon unfolding of the HMCES^{SRAP} adduct. See also Figure S4.

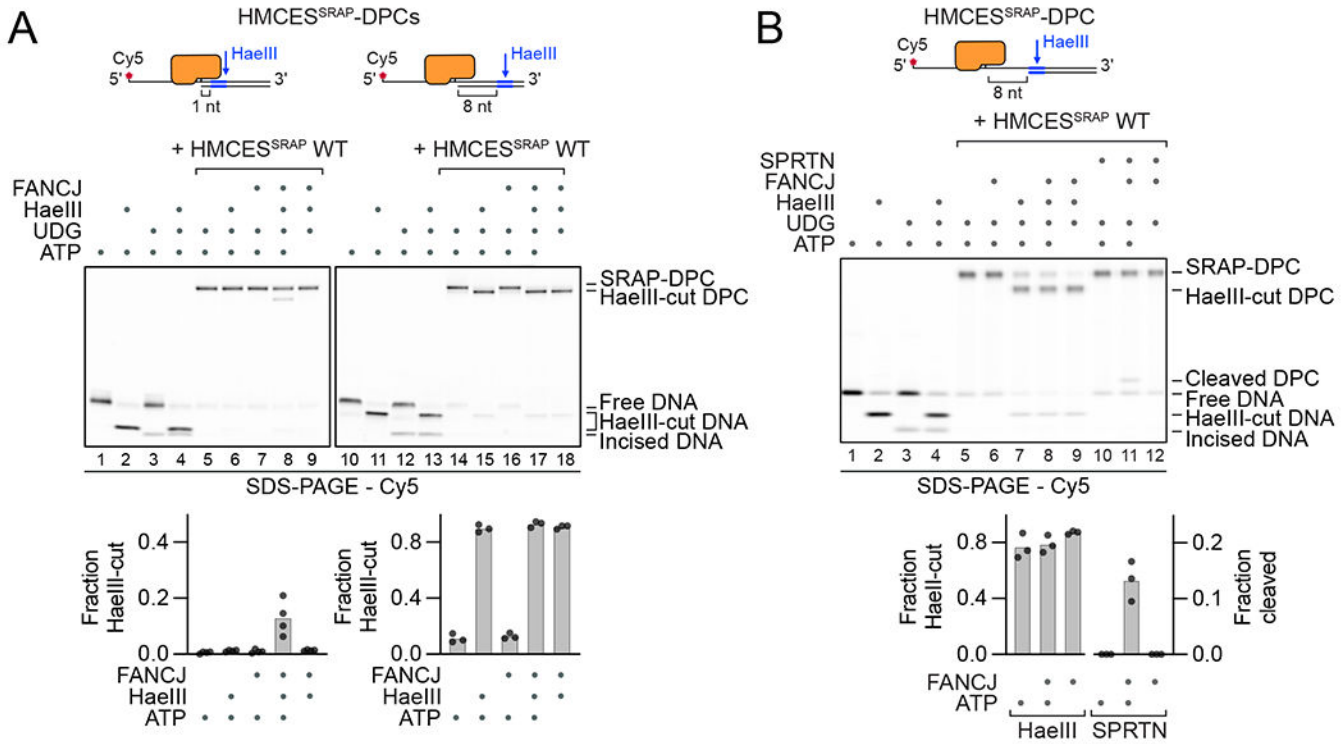

Figure 5. FANCJ exposes DNA underlying the DPC

(A) Analysis of HMCES^{SRAP}-DPC DNA-footprints. Free DNA or the human HMCES^{SRAP}-DPC with HaeIII restriction sites either 1 nucleotide (upper left panel) or 8 nucleotides away (upper right panel) from the DPC position were incubated alone or in the presence of recombinant human FANCJ, HaeIII, and ATP as indicated for 1 h at 37°C prior to separation by denaturing SDS-PAGE. Quantification of HaeIII cutting: bar graph shows the mean of four (lower left panel) or three (lower right panel) independent experiments. **(B)** Free DNA or human HMCES^{SRAP}-DPC next to a recessed junction with a HaeIII restriction site 8 nucleotides away from the DPC position were incubated alone or in the presence of recombinant human FANCJ, human SPRTN, HaeIII, and ATP as indicated for 1 h at 37°C prior to separation by denaturing SDS-PAGE (upper panel). Quantification of DPC cutting by HaeIII or DPC cleavage by SPRTN: bar graph shows the mean of three independent experiments (lower panel). See also Figure S5.

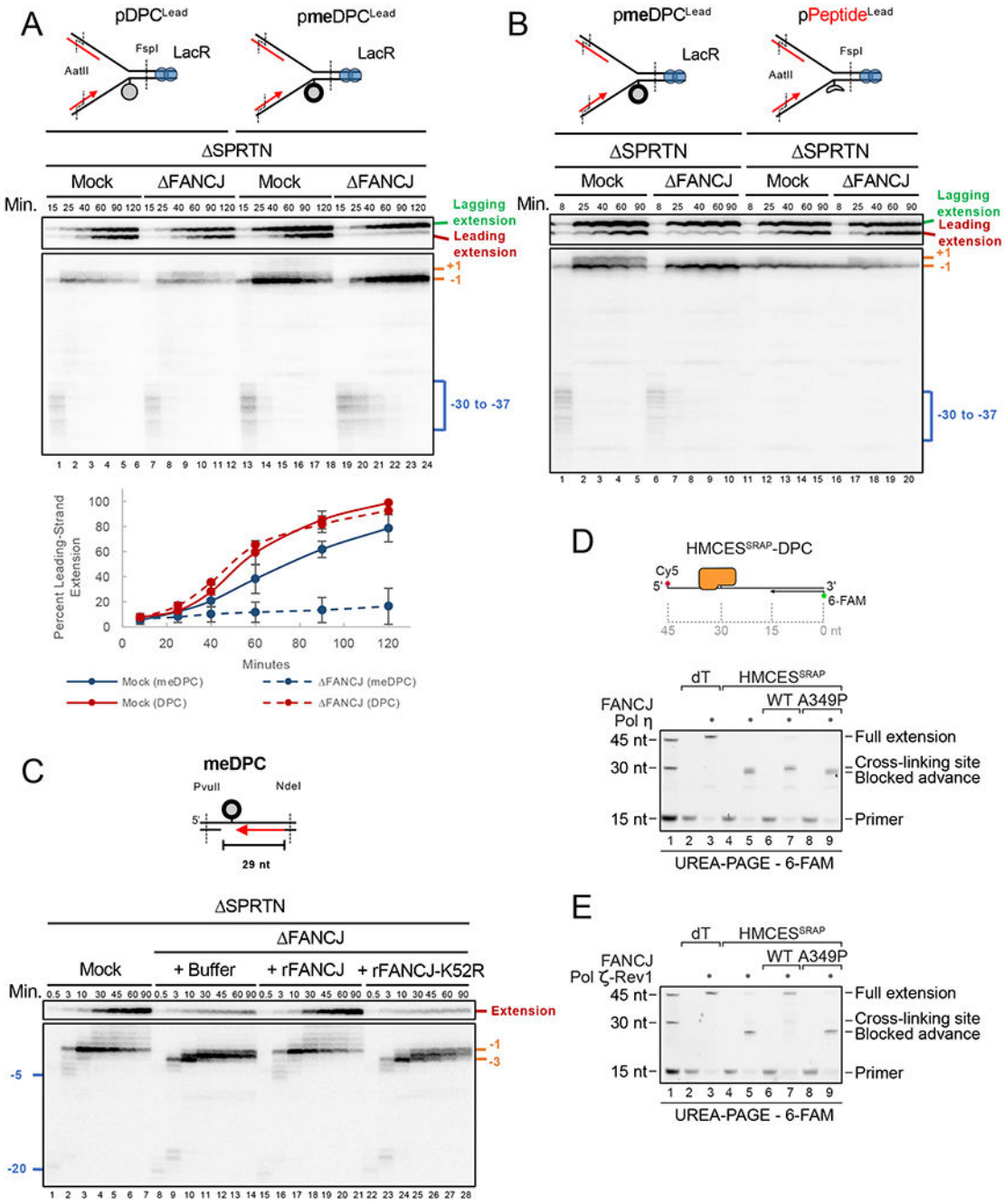

Figure 6. FANCJ is required for translesion synthesis past an intact DPC

(A) The indicated plasmids were pre-incubated with LacR, replicated in the indicated egg extracts containing [α–^{32}P]-dATP, and analyzed as in Figure 1A. **(B)** pmeDPC^{Lead} or pPeptide^{Lead} (generated via proteinase K digestion of pmeDPC^{Lead}) was pre-incubated with LacR, replicated in the indicated egg extracts containing [α–^{32}P]-dATP, and analyzed as in Figure 1A. **(C)** pmeDPC^{ssDNA} was incubated directly in the indicated NPE containing [α–^{32}P]-dATP (analogous to Figure 2D) and supplemented with buffer, recombinant wildtype FANCJ, or ATPase mutant FANCJ-K52R. At different times, DNA was extracted and

digested with PvuII and NdeI, separated on a denaturing polyacrylamide gel, and visualized by autoradiography.

(D-E) Primer extension assay using Pol η and Pol ζ-Rev1. Fluorescently-labelled primer template substrates containing a $HMCES^{SRAP}$-DPC at the indicated position (or dT as control) were incubated alone or in the presence of recombinant human FANCJ (WT or A349P) and recombinant human Pol η (D) or yeast Pol ζ-Rev1 (E) as indicated for 30 min at 37°C prior to separation by denaturing UREA-PAGE.

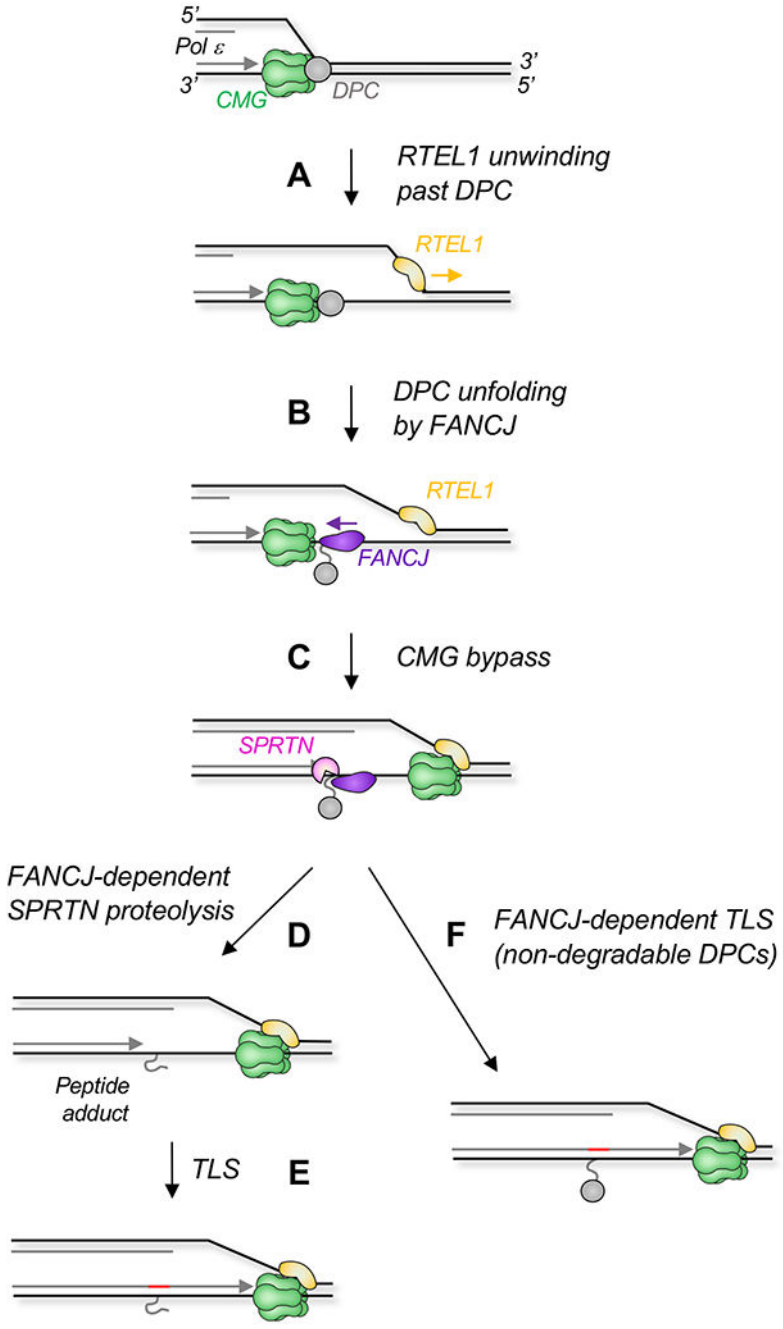

Figure 7. Model for FANCJ's role in DPC repair

(A) Upon replisome collision with a leading strand DPC, RTEL1 (and possibly FANCJ) translocates along the undamaged lagging strand template, exposing ssDNA beyond the DPC, which supports CMG bypass via an unknown mechanism. TRAIP ubiquitylates the DPC before CMG bypass occurs. **(B)** FANCJ loads onto the single-stranded leading strand template downstream of the DPC and translocates back towards the DPC, which it remodels. **(C)** CMG bypasses the DPC. **(D)** After bypass, the DPC undergoes proteolysis by the proteasome or SPRTN, whose activity depends on FANCJ-dependent DPC unfolding. **(E)**

Finally, the leading strand is extended past the peptide. If the DPC fails to be degraded, FANCJ-dependent DPC unfolding enables TLS past the intact adduct **(F)**.

KEY RESOURCES TABLE

REAGENT or RESOURCE	SOURCE	IDENTIFIER
Antibodies		
anti-FANCJ antibody	Novus Biologicals	Cat# NBP1-31883
anti-Actin antibody	Santa Cruz	Cat# sc-47778; RRID: AB_626632
anti-Flag antibody	Sigma	Cat# F3165-.2MG; RRID: AB_259529
anti-xlFANCJ-N	(ref.[35])	Pocono Rabbit Farm and Laboratory Custom Projects 28331 and 28332
anti-xlFANCJ-C	This paper	Bethyl Laboratories Custom Project 61565A
anti-RTEL1-N	J. Walter laboratory, (ref. [14])	Pocono Rabbit Farm and Laboratory Custom Project Pocono 32259
anti-CDC45	J. Walter laboratory, (ref. [36])	Pocono Rabbit Farm and Laboratory Custom Project 534
anti-M.HpaII	J. Walter laboratory, (ref. [6])	Pocono Rabbit Farm and Laboratory Custom Project 31495
anti-PSMA3	J. Walter laboratory, (ref. [6])	New England Peptide Custom Project 3516
anti-SPRTN-N	J. Walter laboratory, (ref. [6])	Pocono Rabbit Farm and Laboratory Custom Project 31053
anti-Histone H3	Cell Signaling	Cat# 9715S; RRID: AB_331563
anti-Mcm6	J. Walter laboratory, (ref. [14])	New England Peptide Custom Project 2926
anti-HMCES	J.Walter laboratory, (ref. [40])	New England peptide Custom Project 4377
Bacterial and virus strains		
BL21 (DE3)	Thermo Scientific	Cat# C600003
Rosetta (DE3) Escherichia coli	MilliporeSigma™	Cat# 70-954-3
Chemicals, peptides, and recombinant proteins		
Triton X-100	Sigma	Cat# T8787-250ML
16% Formaldehyde (w/v), Methanol-free	Thermo Scientific	Cat# 28906
4x NuPAGE LDS sample buffer	Thermo Scientific	Cat# NP0007
smDNAse	Max-Planck-Institute for Biochemistry	N/A
cOmplete EDTA-free protease inhibitor cocktail	Sigma	Cat# 4693132001
DTT	Roth	Cat# 6908.2
His-TEV protease	This paper	N/A
Pefabloc SC	Sigma	Cat# 76307-1G
Biotin	IBA Lifesciences	Cat# 2-1016-005
isopropyl-β-D-thiogalactoside	Sigma	Cat# I6758-10G
Imidazole	Roth	Cat# 3899.1
IGEPAL	Sigma	Cat# I8896-50ML
Protino Ni-NTA Agarose	Fisher Scientific	Cat# 11912422
Tween20	Sigma	Cat# P7949
NaSCN	Sigma	Cat# 467871
Q5® High-Fidelity DNA Polymerase	New England BioLabs	Cat# M0515

REAGENT or RESOURCE	SOURCE	IDENTIFIER
UltraPure BSA	Thermo Scientific	Cat# AM2616
UDG	New England BioLabs	Cat# M0280L
Orange G	Sigma	Cat# O7252-25G
Protein G	BioVision	Cat# 6510
ATP	Thermo Fischer	Cat# R0441
Trypsin Gold	Promega	Cat# V5280
HaeIII	New England BioLabs	Cat# R0108S
dNTPs	New England BioLabs	Cat# N0447S
UREA	Roth	Cat# 3941.3
Ficoll	Sigma	Cat# F4375-25G
Lipofectamine 2000	Invitrogen	Cat# 11668019
Puromycin	Gibco	Cat# A1113803
Q5 Master Mix	New England BioLabs	Cat# M0494L
BP clonase	Thermo Fischer	Cat# 11789020
LR clonase	Thermo Fischer	Cat# 11791100
Hygromycin B	Fisher Scientific	Cat# 10687010
Doxycycline Hyclate	Sigma	Cat# D9891
TCEP	Roth	Cat# HN95.3
HRV 3C protease	Thermo Fisher	Cat# 88947
3XFlag peptide	Sigma	Cat# F4799-4MG
ESF 921 insect cell culture medium	Fisher scientific	Cat# 96-001-01-CS
Nt.BbvcI	New England BioLabs	Cat# R0632L
M.HpaII	J. Walter laboratory, (ref. [5])	N/A
Exonuclease I	New England BioLabs	Cat# M0293S
S-adenosylmethionine	New England BioLabs	Cat# B9003S
[α-^{32}P]-dATP	Perkin elmer	Cat# BLU512H500UC
LacI	J. Walter laboratory, (ref. [5])	N/A
Bromophenol blue	Pharmacia Biotech	Cat# 17-1329-01
Geminin	J. Walter laboratory, (ref. [41])	N/A
Proteinase K	Roche	Cat# 3115879001
RNase A	Sigma	Cat# R4642-250MG
Xenopus RTEL1	J. Walter laboratory, (ref. [14])	N/A
MG262	biotechne	Cat# I-120
1x cutsmart buffer	New England BioLabs	Cat# B7204
Nt.BspQI	New England BioLabs	Cat# R0644S
AatII	New England BioLabs	Cat# R0117L
FspI	New England BioLabs	Cat# R0135L
Formamide	Roche	Cat# 11814320001
Xylene cyanol FF	Sigma	Cat# X4126

REAGENT or RESOURCE	SOURCE	IDENTIFIER
EDTA	Fisher BioReagents	Cat# BP118-500
IgG from non-immunized rabbit serum	Sigma	Cat# R9133-10ML
Protein A Sepharose Fast Flow	GE Healthcare	Cat# 17-1279-03
Streptavidin-coupled magnetic beads	Invitrogen	Cat# 11206D
Usp21	D. Finley lab, and (ref. [42])	N/A
ANTI-FLAG M2 Affinity Gel	Sigma	Cat# A2220-10ML
Nuvia S resin	BioRad	Cat# 1560311
Critical commercial assays		
Q5 site-directed mutagenesis kit	New England BioLabs	Cat# E0554S
Capacity cDNA Reverse Transcription Kit	Thermo Fisher	Cat# 4368814
proFIRE Amine Coupling Kit	Dynamic Biosensors	Cat# PF-NH2-1
T-REx Flp-In system	Thermo Fisher	Cat# K650001
alamarBlue assay	Santa Cruz	Cat# sc-206037A
NucleoSpin® Gel and PCR Clean-up	MACHERY-NAGEL	Cat# 740609.250
Deposited data		
Original western blot and gel images	This paper; Mendeley Data	doi: 10.17632/spdn6vb4wg.1
Experimental models: Cell lines		
Sf21 cells	Thermo Fisher	Cat# 11497013
U2OS T-REx Flp-In	The Francis Crick Institute Cell Services	N/A
Sf9 cells	Expression Systems	Cat# 94-001S
Experimental models: Organisms/strains		
Xenopus laevis	Nasco	Cat# LM0053MX
Oligonucleotides		
Oligonucleotide sequences used in this study are provided in Table S1	N/A	N/A
Recombinant DNA		
pFastBac1-FANCJ -STREP-WT	This paper	N/A
pFastBac1-FANCJ-ZB-STREP-WT	This paper	N/A
pFastBac1-FANCJ-ZB-STREP-A349P	This paper	N/A
pNIC-HIS-SRAP-WT	This paper	N/A
pNIC-HIS-SRAP-C2S	This paper	N/A
pNIC-HIS-SRAP-R98E	This paper	N/A
p11d-tRPA	Addgene	Cat# 102613
pNIC-STREP-ZB-SPRTN-WT	(ref. [16])	N/A
pNIC-STREP-ZB-SPRTN-E112Q	(ref. [16])	N/A
pNIC-STREP-ZB-POLη	This paper	N/A
pX330-Puro	Addgene	Cat# 82580
pDONR221	Thermo Fisher	12536017
pOG44	Thermo Fisher	Cat# K650001

REAGENT or RESOURCE	SOURCE	IDENTIFIER
pcDNA5-FRT/TO-FANCJ-Venus-3xFlag	Addgene	Cat# 17642
pcDNA5-FRT/TO-FANCJ-K52R-Venus-3xFlag	Addgene	Cat# 17643
pcDNA5-FRT/TO-FANCJ-A349P-Venus-3xFlag	This paper	N/A
pcDNA5-FRT/TO-Venus-3xFlag-Gateway	Addgene	Cat# 40999
pMBP-HIS-TEV-protease	This paper	N/A
pJLS2	(ref. [14])	N/A
pJLS3	(ref. [14])	N/A
pJLS102	This paper	N/A
Software and algorithms		
Prism 7	GraphPad Software	https://www.graphpad.com/
ImageJ	NIH	https://imagej.net/Fiji/Downloads
Affinity Designer	Serif	https://affinity.serif.com/de/designer/#buy
Multi-Gauge V3.0	Fujifilm	N/A
Other		
Strep-Tactin® XT 4Flow®	IBA Lifesciences	Cat# 2-5028-001
Superdex® 200 Increase 10/300 GL	GE Healthcare	Cat# GE28-9909-44
HiTrap® Heparin HP	GE Healthcare	Cat# GE17040701
Strep-Tactin® XT Superflow® high-capacity	IBA Lifesciences	Cat# 2-1240-001
HiLoad® 16/600 Superdex® 200 pg	GE Healthcare	Cat# GE28-9893-35
10 kDa cutoff Amicon Ultra centrifugal filters	Merck	Cat# UFC801096
EconoFit Affi-Gel Blue	BioRad	Cat# 12009234
PD-10 Desalting columns	GE Healthcare	Cat# GE17085101